High glucose exposure drives intestinal barrier dysfunction by altering its morphological, structural and functional properties

Nolwenn Dubois, Javier Muñoz-Garcia, Dominique Heymann, Axelle Renodon-Cornière

High glucose exposure drives intestinal barrier dysfunction by altering its morphological, structural and functional properties

Nolwenn Dubois [b], Javier Muñoz-Garcia [a, b],

Dominique Heymann [a, b, c] and Axelle Renodon-Cornière [a, b *]

[a] Nantes Université, CNRS, US2B, UMR 6286, F-44322 Nantes, France.

[b] Institut de Cancérologie de l'Ouest, Tumor Heterogeneity and Precision Medicine Laboratory, 44805 Saint-Herblain, France.

[c] The University of Sheffield, Dept of Oncology and Metabolism, S102RX Sheffield, UK.

* Corresponding author

Dr Axelle Renodon-Cornière: axelle.renodon-corniere@univ-nantes.fr

ABSTRACT

High dietary glucose consumption and hyperglycemia can result in chronic complications. Several studies suggest that high glucose (HG) induces dysfunction of the intestinal barrier. However, the precise changes remain unclear. In our study, we used *in vitro* models composed of Caco-2 and/or HT29-MTX cells in both monoculture and co-culture to assess the effects of long-term HG exposure on the morphological, structural, and functional properties of the intestinal barrier. Cells were grown in medium containing normal physiologic glucose (NG, 5.5 mM) or a clinically relevant HG (25 mM) concentration until 21 days. Results demonstrated that HG induced morphological changes, with the layers appearing denser and less organized than under physiological conditions, which is in accordance with the increased migration capacity of Caco-2 cells and proliferation properties of HT29-MTX cells. Although we mostly observed a small decrease in mRNA and protein expressions of three junction proteins (ZO-1, OCLN and E-cad) in both Caco-2 and HT29-MTX cells cultured in HG medium, confocal microscopy showed that HG induced a

remarkable reduction in their immunofluorescence intensity, triggering disruption of their associated structural network. In addition, we highlighted that HG affected different functionalities (permeability, mucus production and alkaline phosphatase activity) of monolayers with Caco-2 and HT29-MTX cells. Interestingly, these alterations were stronger in co-culture than in monoculture, suggesting a cross-relationship between enterocytes and goblet cells. Controlling hyperglycemia remains a major therapeutical method for reducing damage to the intestinal barrier and improving therapies.

KEYWORDS: high glucose, intestinal epithelium, *in vitro* models, intestinal barrier function; intercellular junction proteins, colorectal cancer.

ABBREVIATIONS: AJ: adherens junctions; ALP: Alkaline phosphatase; CRC: Colorectal cancer; DMEM: Dulbecco's modified Eagle's medium; E-cad: E-cadherin; FR: Fast red TR; HG: High glucose; IE: Intestinal epithelium; MTX: Methotrexate; N: Naphthol AS-MX; N-FR: Naphthol AS-MX and Fast red TR reaction product; NG: Normal glucose; OCLN: Occludin; SD: Standard deviation; TEER: Transepithelial electrical resistance; TJ: tight junctions; ZO: Zonula occludens.

1. INTRODUCTION

Ingestion of high dietary glucose is a risk factor for developing obesity, diabetes and cancer in humans [1–4]. In addition, these diseases are frequently associated with hyperglycemia [2,5]. High dietary glucose consumption and hyperglycemia elevate glucose levels in the blood and many organs and tissues such as the lumen of the intestine. Chronic exposure to high glucose (HG) concentrations can negatively affect these organs and lead to cellular dysfunction that may become irreversible over time.

The intestinal epithelium (IE) is a monolayer composed mainly of two distinct differentiated cell types: enterocytes and goblet cells. It directly interacts with the lumen and acts as a protective barrier against inflammatory molecules such as dietary antigens and pathogens [6–8]. The IE has biological and functional characteristics that can be affected by "pathologies" and dietary factors. Among them, intercellular junctions are a major prerequisite for barrier integrity and are constituted in particular by tight junctions (TJ) and adherens junctions (AJ) [6,9,10]. Key tight junction proteins are occludin (OCLN) and members of the zonula occludens (ZO) family. The major constituent of adherens junctions is E-cadherin (E-cad). The apical side of the enterocytes is distinguished by a brush border which contains several enzymes implicated in gut homeostasis, such as the intestinal alkaline phosphatase [11]. The surface of the IE is covered in a layer of mucus, produced by goblet cells, protecting the host from harmful agents.

For years, the use of human *in vitro* cell models has been a good alternative to *in vivo* studies for reducing the use of animals in research. Different immortalized cell lines have been used to mimic intestinal epithelial cells as they have extended lifespan and decreased experimental variability, while still retaining some of their key functional characteristics. Upon reaching full confluency, the human colon adenocarcinoma Caco-2 cell line spontaneously differentiates to form a polarized cell monolayer, with properties typical of human

enterocytes, such as the tight and adherens junctions and brush border enzyme activities. On the other hand, goblet cells can be mimicked by the HT29-MTX cell line, which is a subpopulation of HT29 human colon adenocarcinoma cells, selected for resistance to methotrexate (MTX), exclusively differentiated into mucus secreting goblet-type cells. These modified cells retain their ability to differentiate under normal culture conditions in the absence of MTX. Therefore, several *in vitro* human intestinal models have been developed using either Caco-2 or HT29-MTX cell lines in either monoculture or co-culture [12–19].

A number of works reported that either chronic or even intermittent exposure of cells to HG induces biochemical and physiological changes that can affect their biological functions [2,20]. The American Diabetes Association defined that a physiological fasting plasma glucose level is around 5.5 mM and that severe hyperglycemia reaches the glucose level of 22.2–25 mM [1]. Consequently, when investigating the influence of glucose on cells, 5.5 mM glucose (1 g/L) in the media corresponds to normal physiological levels (NG), whereas 25 mM (4.5 g/L) is considered to be the high glucose (HG) concentration [1,21–27]. Several studies have highlighted that HG modulated multiple signalling pathways may contribute to proliferation, migration, invasion and/or recurrence of cells from various tissues [5,24,28–31]. Some of these studies suggested that HG markedly interfered with homeostatic intestinal epithelial integrity, damaging intestinal barrier functions, and increasing intestinal permeability. Impaired intestinal barrier function may result from a combination of events affecting the properties of the tight and adherens junctions, the mucus layer and/or the brush border enzyme activities. Some of these IE characteristics have been partially investigated. Accordingly, it has been shown *in vitro* that HG resulted in increased proliferation [26,28,32–34], migration [28,33,35] and reactive oxygen species production [32,33,36], and decreased transepithelial electrical resistance with increased membrane permeability [21,23,36,37]. In a few cases, expressions of intercellular junctional proteins have been investigated at the

4

mRNA and/or protein levels [28,35–37] and/or their subcellular locations have been examined [23,30,38]. Limited studies have assessed the effects of HG on IE barrier functionality, such as mucus secretion or ALP activity and they have mostly been done *in vivo* [26,37,39,40]. Thus, how excessive glucose ingestion as part of a long-term diet impacts the IE still needs to be understood.

The aim of the study was to explore *in vitro* the effects of the glucose concentrations corresponding to physiological and hyperglycemia conditions on various functional and structural characteristics of the two main cell types representing the IE, enterocytes (Caco-2) and goblet cells (HT29-MTX). This study provides important information regarding the impact of prolonged hyperglycemia exposure on the human intestinal barrier and the involvement of chronic disease development.

2. MATERIALS AND METHODS

2.1. Cells and reagents

Caco-2 (Cat. #86010202) and HT29-MTX (Cat. #12040401) cell lines were obtained from the European Collection of Authenticated Cell Cultures (ECACC, Salisbury, UK). FITC-dextran (10 kDa), Alcian blue, fast Red TR/Naphthol AS-MX Tablets, non-essential amino acids (NEAA), bovine serum albumin, Igepal, sodium dodecyl sulfate (SDS), glycerol, triton X-100 and sodium deoxycholate were provided by Sigma-Aldrich (Saint-Quentin-Fallavier, France). Acrylamide/Bis-Acrylamide (37.5:1) 30% solution was obtained from Euromedex (Souffelweyersheim, France). Dulbecco's Modified Eagle's Medium with phenol red (DMEM), high glucose and low glucose, penicillin/streptomycin, L-Glutamine 200mM 100X, and all solvents, were obtained from Dutscher (Brumath, France). Sodium chloride, Tris-(hydroxymethyl) aminomethane (TRIS, Trometamol) ≥ 99.9% were purchased from VWR (Fontenay/Bois,France). Foetal bovine serum (FBS) was obtained from Eurobio (Les-Ulis, France). Halt™ Protease Inhibitor Cocktail (100X) was purchased from Fisher scientific (Saint Aubin, France). Tris-glycine-SDS buffer, tris-glycine buffer, bio-safe Coomassie, and clarity Western ECL were obtained from Biorad (Marnes-la-Coquette, France). All antibodies used for Western blot and immunofluorescence staining were purchased from Cell Signaling (Ozyme, Saint Quentin en Yveline, France).

2.2. Cell culture conditions

The human colon adenocarcinoma Caco-2 and HT29-MTX cell lines were used in experiments at passages between P10 and P22. After thawing, cells were maintained separately in a flask in high glucose DMEM (HG = 4.5 g/L, 25 mM) and low glucose DMEM (NG = 1 g/L, 5.5 mM) culture media. Each culture medium was supplemented with 10% (v/v) heat inactivated FBS, 1% (v/v) NEAA, 1% (v/v) L-glutamine and 1% (v/v) penicillin and

streptomycin. Cells were grown at 37°C in a 5% CO_2 humidified atmosphere with changes of media every 2-3 days. Cells were never cultured above 80% confluency, and all cell lines were periodically checked for the presence of mycoplasma.

2.3. Transepithelial electrical resistance (TEER)

For this experiment, 12-well polycarbonate Transwell inserts with a 6.5 mm diameter and 0.4 µm pore size (Corning, NY, USA) were used. Caco-2 and HT29-MTX cells were counted by Malassez cells. The cells were then mixed in a population ratio Caco-2:HT29-MTX cells of 1:0, 9:1, 8:2, 7:3 or 0:1 and seeded into apical chambers with a final density of 1.5 x 10^5 cells/cm² in each insert. 100% of cell confluency was reached between days 1 and 2. Cells were cultured for 21 days, with two culture medium conditions (NG and HG), under the same conditions as previously described. The medium (200 µL in the apical chamber and 900 µL in the basolateral chamber) was refreshed every 2-3 days. The assessment of the transepithelial electrical resistance (TEER), was carried out using the Millicell ERS-2 electrical resistance system at Millipore (Merck, Darmstadt, Germany). TEER was used to check integrity and monolayer formation for 21 days before experiments. Twice a week, TEER measurement was performed by placing electrode tips into two chambers in each Transwell insert. The results are expressed in ohms/cm² after subtracting the blank value from an insert without cells.

2.4. Permeability assay

At 18 days post seeding, culture medium was aspirated and 200 µL of FITC-dextran (10 kDa), diluted in the corresponding medium (NG or HG) at 1 mg/mL, were added to the apical chamber of each monolayer. In the basolateral chambers, 900 µL of the corresponding medium (NG or HG) were added and the plates were incubated at 37°C in 5% CO_2. Samples (100 µL) were collected after 2h, 4h, 6h and 24h from the basolateral chambers, transferred to

a black 96-well plate, and replaced by the same amount of medium. FITC-dextran quantification was performed by measuring fluorescence at an excitation wavelength of 485 nm and an emission wavelength of 535 nm on a Victor X3 Multimode Microplate Reader (Perkin Elmer, Waltham, MA, USA).

2.5. Mucus staining

At 21 days post seeding, mucus secreted by HT29-MTX cells cultured on Transwell was stained using Alcian blue. Briefly, culture medium was aspirated and the cells were fixed with cold Carnoy solution (60% ethanol, 30% chloroform, 10% acetic acid) in both apical and basolateral compartments for 15 min at room temperature, then washed once with 1X PBS 3% acetic acid. Carnoy solution was used to preserve the mucus layer. Alcian blue solution was added to the apical compartment at room temperature for 15 min and washed three times with cold PBS. After washings, polycarbonate membranes were removed using a scalpel blade, transferred on to a slide, and mounted with coverslips using gold anti-fade mounting reagent (Invitrogen, Cergy-Pontoise, France). The mounting agent was allowed to set overnight prior to analysis using light microscopy at 2X magnification. Images were taken with a Nikon digital camera mounted on a Nikon Eclipse Ni microscope (Nikon instrument, Japan) processed by NIS-Elements (BR). The blue stained surface, corresponding to mucus layer formation at the monolayer surfaces, was estimated with ImageJ software, version 1.53T (NIH, Bethesda, USA).

Mucus production by HT29-MTX cells also underwent histochemical analysis. After removal, polycarbonate membranes were dehydrated, and embedded in paraffin prior to performing 3 µm cross sections. After hematoxylin/eosin and Alcian blue staining, slides were scanned on Nanozoomer S60 (Hamamatsu photonics, Hamamatsu City, Japan) and analyzed using NDP viewer 2 software (Hamamatsu photonics, Hamamatsu City, Japan).

2.6. Alkaline phosphatase assay

ALP that was expressed only on the brush border of differentiated Caco-2 cells was examined with Fast-Red TR/Naphthol AS-MX staining. Caco-2 and HT29-MTX cells were seeded in monoculture or co-culture with different ratios (9:1, 8:2, 7:3 respectively) on Cell Carrier^{TM} 96 ultra-well plate (Perkin Elmer, Waltham, MA, USA) with a density of 1 x 10^4 cells/well, that reached 100% of cell confluency between days 3 and 4. Cells were grown with two culture medium conditions (NG and HG), at 37°C in 5% CO_2 and moisture to make possible cellular differentiation and the development of microvilli for 7, 14, and 21 days. Before coloration, brightfield images of each well were acquired using the Operetta CLS^{TM} high throughput microplate imager (5X magnification) to visualize the monolayer's morphology. Confluent cells, at days 7, 14, or 21 post seeding, were washed once with cold PBS. Fast-Red TR/Naphthol AS-MX solution was added to monolayers without prior fixation of cells, then incubated 30 min at 37°C in the dark room. Supernatant was recovered, and absorbance was measured to 525 nm on a Victor Nivo Multimode Microplate Reader (Perkin Elmer, Waltham, MA, USA).

2.7. Cell migration measurement by means of a scratch test

Caco-2 and HT29-MTX cell motilies were studied with a scratch assay, which measures the expansion of a cell population on surfaces. Cells were seeded on 12-well plates with a density of 3.1 x 10^4 cells/cm² for Caco-2 cells and 3.7 x 10^4 cells/cm² for HT29-MTX cells, with two DMEM culture medium conditions (NG and HG). These seeding densities were chosen to achieve 100% of cell confluency by day 3. 3 days post seeding, monolayers were manually scratched with a 200 µL pipette tip to create a linear wound in the centre of each well. Detached cells were removed by washing the monolayer twice with PBS. Each condition was

performed in triplicate. Cells were cultured at 37°C, in 5% CO_2, and a series of 48 frames per well were acquired using a 5X magnification on the Operetta high-content imaging system (Perkin Elmer, Waltham, MA, USA) every day for 4 days. Scratch wound healing was estimated by evaluating the cell expansion area using ImageJ software. Data were expressed as the distance covered by the cells (mm) after the wound had occurred.

2.8. Cell growth assay

Serial measurements of cell numbers were carried out to establish growth curves of Caco-2 and HT29-MTX cells in various conditions. In order to be able to follow the increase in cell numbers over several days before reaching cell confluency, Caco-2 and HT29-MTX cells in monoculture were seeded on 6-well plates with a density of 6.6 x 10^3 cells/cm² in the volume of 3 mL using two DMEM culture medium conditions (NG and HG). Every 2-3 days, cells of one well were harvested in 500 mL trypsin/EDTA and counted using a Malassez cell.

2.9. Western blot analysis.

Protein expressions in Caco-2 and HT29-MTX cell monolayers were determined by Western blot analyses. Cells in monoculture were seeded on 6-well plates with a density of 3 x 10^4 cells/cm² in the volume of 3 mL using two DMEM culture medium conditions (NG and HG). 100% of cell confluency was reached between days 3 and 4. At 7, 14 and 21 days post seeding, the medium was removed, cells were washed twice with PBS and directly scraped using 150 µL of lysis buffer per well (RIPA: 150 mM NaCl, 1% Igepal, 50 mM Tris-HCl (pH 7.4), 1 mM EDTA, 0.5% sodium deoxycholate, and 0.1% SDS), containing a protease inhibitor cocktail (#1862209, Thermo scientific, Saint Aubin, France), and kept at -80°C before protein extraction.

For total protein extraction, Caco-2 and HT29-MTX samples were incubated on ice for 60 min and centrifuged at 2×10^4 g for 20 min at 4°C. Supernatants were collected and protein concentrations were evaluated using a BC Assay quantitation kit (Interchim SA, Montluçon, France), according to the manufacturer's instructions using bovine serum albumin as standard. Equal amounts of proteins (30 μg) were diluted in water, and 4X blue electrophoresis buffer (250 mM Tris–HCl pH 6.8, 10% 2-mercaptoethanol, 8% SDS, 40% glycerol and 0.04% bromophenol blue), boiled for 10 min at 95°C, and separated by SDS-PAGE with 10% polyacrylamide gel. The separated proteins were transferred to Immobilon Transfer polyvinylidene fluoride membranes from Millipore (Merck, Darmstadt, Germany). Blots were blocked with 5% BSA in TBS-0.1% Tween (TBST) and the membranes were incubated overnight at 4°C using the following primary antibodies: rabbit monoclonal occludin antibody (1:2000; Cat. #91131, Cell Signaling), rabbit monoclonal ZO-1 antibody (1:2000; Cat. #8193, Cell Signaling), or rabbit monoclonal E-cadherin antibody (1:2000; Cat. #3195, Cell Signaling). Then, an anti-rabbit horseradish peroxidase (HRP)-conjugated secondary antibody (1:10000; Cat. #7074S, Cell Signaling) was incubated for 1 h at room temperature.

After several washings using TBST, the membranes were exposed on a Chemidoc MP imaging system (Biorad, Marnes-la-Coquette, France) with ECL to detect antibody binding. Peroxydase activity was recorded and analyzed by using Image Lab version 5.0 software (Biorad, Marnes-la-coquette, France). To quantify the intensities of the stained bands for normalization, we used housekeeping protein β-actin, which was detected by a rabbit monoclonal β-actin antibody (1:10000; Cat. #4970, Cell Signaling).

2.10.   RNA isolation and quantitative PCR (RT-qPCR)

The mRNA expressions of various genes in Caco-2 and HT29-MTX cells were explored using qPCR. Cells in monoculture were seeded on 6-well plates with a density of 3×10^4

cells/cm² in the volume of 3 mL using two DMEM culture medium conditions (NG and HG). At 2, 7, 14, and 21 days post seeding, the medium was removed, cells were washed twice with PBS and directly scraped using 150 µL of RA1 lysis buffer (from the RNA extraction kit, see below) per well. Supernatants were transferred to tubes and kept at -80°C before RNA extraction. Total RNA was extracted using a Nucleospin RNA kit (Macherey-Nagel, Hoerdt, France), according to the manufacturer's instructions. The concentration of total RNA was determined by absorbance at 260/280 nm using a NanoDrop™ one spectrophotometer (Thermo scientific, Saint Aubin, France). Reverse transcription was carried out with 1 µg of total RNA using QuantiTect Reverse Transcription Kit (Qiagen, Hilden, Germany), according to the manufacturer's instructions.

PCR amplification was carried out on Rotor Gene Q (Qiagen, Hilden, Germany), with 25 ng of cDNA (5 µL) in 15 µL of reaction mixture containing 10 µL of Power up SYBR Green master mix (Applied Biosystems, Life Technologies), and 5 µL of forward and reverse primers (2 µM), for each sample. The qPCR conditions were as follows: an amplification phase at 95°C for 5 min followed by 40 cycles at 95°C for 5 s and 60°C for 10 s. Finally, melt curve analysis was performed by gradually increasing the temperature from 60°C to 95°C to verify that each of the chosen primer pairs amplified a single product with a distinct melting temperature. The primer sequences used for quantification of ZO-1, OCLN and E-cad are shown in Table 1. ß-Actin was used as the housekeeping control gene. The gene expression was compared to the housekeeping gene, using the $2^{-\Delta\Delta CT}$ method.

2.11. Immunofluorescent staining

Caco-2 and HT29-MTX cells in monoculture were seeded on Cell Carrier™ 96 ultra-well plates (Perkin Elmer, Waltham, MA, USA), with a density of 1×10^4 cells/well. Cells were grown during 7, 14, and 21 days with two DMEM culture medium conditions (NG and HG).

Before immunofluorescence staining, brightfield images of each well were acquired using the Operetta CLS™ high throughput microplate imager (5X magnification) to visualize the monolayer morphology.

Confluent cells at days 7, 14, or 21 post seeding were washed once with PBS, fixed with 4% paraformaldehyde for 20 min, then washed once with PBS. Permeabilization was performed with 0.1% Triton X-100 in PBS for 10 min at room temperature. Cells were washed once with PBS before incubation for 1 h in PBS-BSA 3% blocking buffer.

Monolayers were incubated overnight at 4°C using the same primary antibodies as the Western blot analysis: rabbit monoclonal occludin antibody (1:600), rabbit monoclonal ZO-1 antibody (1:200) or rabbit monoclonal E-cadherin antibody (1:600). Subsequently, after washings using PBS, monolayers were incubated with Alexa Fluor 488 anti-rabbit IgG (1:1000; Cat. #4412S, Cell Signaling, USA), with Alexa fluor 647 phalloidin (1:40; Cat. #8940S, Cell Signaling), 1 h at room temperature, in the dark. All antibodies were diluted in PBS-3% BSA. Cells were washed twice with PBS for 5 min, then the nuclei were stained with DAPI for 10 min during the last wash. A final wash was performed with PBS for 5 min. Fluorescence microscopy images were captured under 63X magnification on the Operetta high-content imaging system and analyzed using Harmony 4.9 software.

2.12. Statistical analysis

Results are expressed as the mean ± standard deviation (SD). Statistical analyses were performed using two-way ANOVA with Tukey's multiple comparisons test using GraphPad Prism software version 6.0 for Windows (GraphPad Software, San Diego, CA). Differences with a p-value < 0.05 were considered statistically significant.

3. RESULTS

3.1. Effect of HG on the growth of Caco-2 and HT29-MTX cells

Glucose is an important source of energy and nutrients for the growth and survival of normal and cancer cells. To test the impact of glucose on intestinal cell growth, Caco-2 and HT29-MTX cells, which constitute *in vitro* models of the two main intestinal cell types (respectively enterocytes and goblet cells), were incubated in culture media containing two concentrations of glucose [normal glucose (NG, 5.5 mM) and high glucose (HG, 25 mM)]. Cells were maintained in the corresponding medium for at least three passages before the experiment but no more than 15 passages (to avoid the selection of distinct cell populations). This separate growth of cells in NG or HG condition prior experiments allows us to compare whether the behavior of these cells differs when they are routinely grown in the different medium, in correlation with the effects of a long-term glucose-rich environment on the functions of the intestinal barrier. Cell numbers were determined for 14 days after seeding. The growth curves showed typical characteristics for the two cell lines. Briefly, a short lag phase was followed by an exponential growth phase (day 3 to day 10). The curves ended with a plateauing of cell density. We observed that there was no significant difference in glucose concentrations for Caco-2 cell proliferation (Fig. 1A) whereas HG increased the cell growth of HT29-MTX cells compared to normal glucose conditions (Fig. 1B). The number of cells at confluency was higher in HG medium compared to NG medium. This result suggests that the cells may have a different morphology depending on the medium used.

3.2. Effect of HG on membrane integrity and permeability in Caco-2 and HT29-MTX cell monolayer in monoculture

To evaluate the effect of HG on membrane integrity, TEER measurements can be monitored in intestinal cell monolayers grown on a Transwell membrane. Since we worked under long-

term exposure conditions, glucose concentration was similar in the apical and basolateral compartments, either NG or HG. As shown in Fig. 2A, TEER values of both cell lines increased progressively with time until a maximum around day 18. The TEER across Caco-2 cells was higher than that across HT29-MTX cells. The average TEER of both cell lines had the highest level in NG medium, suggesting that HG decreased membrane integrity. In addition, apical to basolateral fluxes of FITC-dextran (10 kDa) were measured to assess the monolayer permeability. These fluxes increased as a function of time between 2h and 24h for both cell lines (Fig. 2B and 2C). The results are consistent with those obtained from TEER measurements, with a higher permeability of HT29-MTX cell monolayers compared with the Caco-2 cell monolayers. Significant increases in permeability were observed in the presence of HG medium for both cell lines at 24h ($p < 0.001$), and as early as 4h for HT29-MTX cells ($p < 0.01$). Nevertheless, these dextran permeabilities are very low with, respectively for HT29-MTX and Caco-2 cells, values $< 2\%$ and $< 0.4\%$ at 6h and $< 10\%$ and $< 0.5\%$ at 24h. Consequently, barrier properties restricting permeability appears to be less developed in the HG condition.

3.3. Effect of HG on Caco-2 and HT29-MTX cell monolayer morphology

To investigate whether HG exposure affects monolayer formation, we compared morphological features of IE cells grown in NG or HG medium. Brightfield images of the Caco-2 and HT29-MTX cells cultured on 96-well plates were taken at 3 different days of culture after seeding (days 7, 14 and 21). We observed differences between monolayers in their general appearance during growth. Cells grew rapidly in confluent flat monolayers (Fig. 3). For Caco-2 cells, dark spots were already observed on the monolayers on day 7 in both media. In addition, in some places, the monolayer became very dense and three-dimensional, forming domes. These elevations have been previously described and are correlated to cell

differentiation and transepithelial transport. These observations indicated that the cells maintain their polarization capacity *in vitro* and display directed salt and water transport as well as strong cell to cell contacts, forming a water-impermeable layer [41]. At day 7, the monolayers looked similar between the NG and HG media. Differences appeared over time with a density that seemed slightly higher in HG medium than in NG medium at day 21. These results suggest that the cells were growing on top of each other in HG medium. Differences over time appeared to be more pronounced for HT29 than for Caco-2 cells with much denser monolayers in HG medium than in NG medium.

In addition, we investigated the morphological changes in cell nuclei using DAPI staining, which supported that HG induced modifications in the nuclear morphology for both Caco-2 and HT29-MTX cells (Fig. 4). HG decreased the nucleus area and fluorescence intensities. For HT29-MTX, increased numbers of nuclei per well were found at days 7 and 21, which is in line with the increase observed in cell growth and number of cells at confluency (Fig. 1B). These results confirm that the cells cultured in the two media have different morphologies.

3.4. Effect of HG on Caco-2 and HT29-MTX cell migration capacity

Cell motility is a hallmark of many gut-related physiological and pathological processes such as wound repair and cancer metastasis. Thus, to determine the influence of glucose on cell migration, we performed a wound healing assay, which provides an indirect measurement of the ability of IE cells to repair mucosal injury and maintain the integrity of the intestinal barrier. The closure of a scratch applied to confluent cell monolayers was monitored for 96 h. As shown in Fig. 5, the wound closure increased with time for all the conditions. The migration was significantly faster with Caco-2 compared to HT29-MTX cells. Data are expressed as the distance covered by the cells in mm after the wound had occurred. This distance was not dependent of the width of scratches. In order to get a visual effect of wound

closure in Fig. 5A, larger scratch widths (at 0h) were chosen for Caco-2 cells than for HT29-MTX cells. The results demonstrated that Caco-2 cells cultivated in HG medium migrated at a faster rate than in NG medium (Fig. 5A and 5C). In contrast, HT29-MTX cells did not appear to migrate differently with glucose concentrations (Fig. 5B and 5D).

3.5. Effect of HG on protein junction expression and localization in Caco-2 and HT29-MTX cell monolayers in monoculture

To assess whether more subtle cellular morphological changes than those measured by TEER and observed by microscopy can occur, changes in junctional protein expression and localization were evaluated. We were particularly interested in tight junction (ZO-1 and OCLN) and adherens junction (E-cad) proteins. These proteins play an important role in maintaining cellular barrier functions [6,9,10]. Cell monolayers were cultured in NG or HG medium for 7, 14 or 21 days. Then either mRNA or protein contents were extracted, and their levels were quantified with RT-qPCR and Western blotting respectively.

As shown in Fig. 6, mRNA expression levels of all proteins increased with time, in accordance with the progressive constitution of monolayers. For the most part, in Caco-2 cells, mRNA expression levels of all proteins were slightly reduced in the HG condition compared with the NG condition (Fig. 6A). In contrast, for HT29-MTX cells, although the expression levels of E-cad were also reduced in HG medium at day 21, the mRNA levels of ZO-1 and OCLN were similar or slightly higher (Fig. 6B). It is important to note that the variations in mRNA expressions between NG and HG media were low (mostly < 1.5-fold).

Concerning protein expression levels, for Caco-2 cells, Western blot quantification demonstrated that HG did not cause any notable change in protein expressions (Fig. 7A and 7C). Nevertheless, even though the differences were not statistically significant, slightly lower protein content was frequently observed in samples grown in HG medium at any time

considered for most of the proteins studied, except for ZO-1 at D21. We noticed decreases in the detected amount of ZO-1 as the culture time increased in both media ($p < 0.01$). For HT29-MTX cells, results were depending on the protein and time of interest (Fig. 7B and 7D). While we observed lower OCLN content at D7 ($p < 0.001$) in HG medium compared to NG medium, the variations were not significant for E-cad, OCLN at D14 and D21 and ZO-1 at D7. Intriguingly, we found a clear decrease in the detected amount of ZO-1 in NG medium as the culture time increased ($p < 0.0001$). ZO-1 was thus barely detectable in the HT29-MTX monolayer developed in NG medium at days 14 and 21. More protein was detected on these same days in the HG condition, indicating that HG maintained ZO-1 levels at a fairly high content with time while it was reduced in NG medium. It should be noted that the anti-ZO-1 antibody used in this work recognizes the two protein isoforms but our Western blot conditions did not enable us to separate them. We also observed that while the amount of OCLN decreased slightly with time in NG medium, it increased in HG medium ($p < 0.01$).

Next, we assessed the effect of HG on the cellular localization of these junction proteins by using immunofluorescence staining. We noticed that ZO-1, OCLN and E-cad all exhibited the typical intercellular network with continuous immunolocalization encircling the individual cells. Interestingly, the intensities of the ZO-1, OCLN and E-cad signals of both types of IE cell were markedly reduced in monolayers cultured in HG medium compared to NG medium, especially at days 14 and 21 (Fig. 8). In addition, for HT29-MTX cells, immunofluorescence localization of ZO-1, OCLN and E-cad, especially at day 21, indicated that HG induced modifications in the morphological shape of the cells. Signals were more localized at the intercellular junctions and the network seemed tighter. This result was in agreement with nucleus immunofluorescence staining, showing lower signal intensities and an increased number of nuclei in HG medium (Fig. 4B). In accordance with Western blot analysis, we found a time-dependent decrease in the presence of protein for ZO-1 in Caco-2 and HT29-

MTX cells. We did not see any notable variation with time in the immunofluorescence intensities of OCLN and E-cad in either medium.

Confocal X-Z images were generated to visualize the localization of the corresponding proteins in the Z planes (Fig. 8C and 8D). For both cell types, they revealed that OCLN and E-cad was mainly localized in the lateral membranes and ZO-1 was focused at the apical side of the lateral membranes. These images also confirmed that HG induced morphological and structural differences in the monolayers. The image analysis parameters were chosen to correctly visualize the signals. It is important to note that the signal intensities in the HG medium were lower than those in the NG medium for Caco-2 and HT29-MTX cells, reinforcing what has been seen previously (Fig. 8A and 8B). Moreover, for Caco-2 cells in HG medium, a few spots of ZO-1 were focused a little more towards the basolateral side on the lateral membrane. Furthermore, distribution of OCLN and E-cad along the lateral membranes highlighted that the monolayer appears thinner in NG medium compared to HG medium for both IE cells (Fig. 8C). It is also worth noting, for Caco-2 cells, that we found that these structural and morphological changes were not observed in NG medium containing 20 mM of mannitol (data not shown). The use of mannitol allows us to exclude potential hyperosmotic effects that may arise due to high glucose. For HT29-MTX cells, the experiments could not be performed as 20 mM of mannitol appeared to be toxic to cells that detached from the culture support. Immunofluorescence staining via phalloidin of F-actin, a key marker of the cytoskeleton, was also performed and did not show any significant variations between NG and HG media (data not shown).

Taken together, our results demonstrated that HG-induced impairment of the intestinal barrier led to both density changes and redistribution of intercellular junction proteins, and morphological modifications in the IE cells. These structural alterations may impact the functional characteristics of the barrier such as mucus production and ALP activity.

3.6. Effect of HG on the mucus production of Caco-2 and HT29-MTX cell monolayers in monoculture

Mucus production, a major function of the IE, was then examined for both medium conditions and cell types. Secreted mucus along the monolayers was evaluated using Alcian blue, a cationic dye which specifically binds to acidic mucin glycoproteins, leading to a deep blue colour. As indicated previously, Caco-2 cells showed only background levels of staining, confirming that they are not able to produce mucus (Fig. 9A and 9B). On the other hand, Fig. 9 shows that mucus was successfully produced by HT29-MTX cells. We did not find any significant variation in mucus production between NG and HG conditions, as 100% of the insert surface was covered in both conditions. Nevertheless, a slight increase in the intensity of the mucus stain could be observed in the presence of HG medium (Fig. 9A). In addition, histological examination of paraffin-embedded vertical cross sections of the HT29-MTX monolayer stained with Alcian blue confirmed that no increase in the thickness of the adherent mucus layer seemed to appear by culturing the cells in HG medium compared to NG medium. It also confirmed that HT29-MTX cells grown in NG medium displayed a well-polarized monolayer, whereas the same cells grown in HG medium showed a less organized pattern and appeared to be pseudo-stratified or even multi-layered at several locations along the entire layer on the insert.

3.7. Effect of HG on the ALP activity of Caco-2 and HT29-MTX cell monolayers in monoculture

ALP activity reflects microvilli development and indicates the correct differentiation of enterocytes. Here we developed a new colorimetric method to validate the differentiation and functionality of the barrier by measuring ALP activity using the coupling reaction of naphthol

AS-MX (N) and fast red TR (FR) as substrates. The UV-visible absorption spectrum of the corresponding reaction product (N-FR) between 350 and 600 nm showed two maximum peaks around 525 and 565 nm (data not shown). The amount of N-FR produced was proportional to the change in absorbance at 525 nm and to ALP activity. This method was applied to the cell monolayers formed on 24-well Transwell membranes and 96-well plates. Both cell culture supports showed similar results (data not shown), indicating that they allow faithful differentiation of the monolayers.

The ALP activities of the HT29-MTX monolayers were close to the background noise level and did not vary with time (Fig. 10). For the Caco-2 monolayers, ALP activities increased progressively from day 7 to day 21 (Fig. 10). We did not observe any significant variation between NG and HG media, suggesting that HG did not affect the differentiation of Caco-2 cells and their microvilli formation.

3.8. Effect of HG on the functional characteristics of Caco-2 and HT29-MTX cells in co-culture

To improve the Caco-2 cell model for simulating human intestines, co-cultures of Caco-2 cells with HT29 cells were frequently established [12–19]. The characteristics of these co-culture models are closer to those of the human small intestine. Depending on the studies, the proportions of the two cell types in co-culture vary and several authors have investigated the optimal cell ratio. Using EGFP-transfected Caco-2 cells, Araujo and Sarmento indicated that, after 21 days in culture, the 9:1 proportion resulted in around 95% of EGFP positive Caco-2 cells, the 8:2 proportion around 93% and the 7:3 proportion, around 90% [13]. They finally elected to work with the 9:1 ratio which is the most commonly used ratio in the literature [13,16,17]. Nevertheless, many authors have chosen other ratios, such as 8:2 [12,14,42] or 7:3

[15,18,19,43]. In any case, it is worth noting that in our experiments, we were unable to specify precisely the ratio of Caco-2 versus HT29-MTX cell numbers at each culture time.

We investigated three barrier functions of Caco-2 and HT29-MTX cell monolayers in co-culture with three ratios (9:1, 8:2 and 7:3): mucus production, ALP activity and permeability by TEER and FITC-dextran flux measurements. First, the blue staining area of the different co-cultures increased with the ratio of HT29-MTX cells (Fig. 11A and 11B). Under these conditions, we found a more intense blue staining of the co-culture monolayers in HG medium, compared to NG medium. Ultimately, HG slightly increased the mucus production ability of HT29-MTX cells, and thus goblet cells. Second, we found similar ALP activities between Caco-2 monolayers in monoculture and in co-culture with HT29-MTX cells (Fig. 11C). ALP activities gradually increased from day 7 to day 21 for all co-culture monolayers. HG tended to decrease ALP activity a little, but differences were low and not significant in our experimental conditions, indicating that HG may not have a drastic impact on enterocyte activity.

Finally, when the ratio of Caco-2 cells decreased in the co-culture monolayers, TEER values also decreased (Fig. 11D, $p < 0.001$) and the FITC-dextran fluxes increased (Fig. 11E, $p < 0.0001$). This is in line with the results of the monoculture monolayers where Caco-2 cells exhibited a high TEER and a low FITC-dextran permeability while HT29-MTX cells displayed a low TEER and a higher FITC-dextran permeability than Caco-2 cells. We showed that HG affected the permeability properties of the co-culture monolayers by significantly decreasing the TEER, which measures the ion flux through the barrier and increasing apical to basolateral flux of FITC-dextran. This increase in permeability implies a decrease in barrier integrity induced by HG. Taken together, our results highlighted that HG strongly impacts the properties of the intestinal barrier by modulating its functionalities.

4. DISCUSSION

The prevalence of excess weight and obesity in the United States and Europe has climbed almost unabated in the last 50 years, leading to an increase in chronic diseases such as cancer, cardiovascular disease, type 2 diabetes, hypertension and coronary heart disease [1–4]. The role of diet and physical activity in mitigating the risk of obesity have gained much attention, justifiably, given that deaths can increasingly be attributed to excess weight, caused by poor diet and physical inactivity [3,8,44,45]. Overweight people tend to ingest glucose-containing foods, which can lead to glucose addiction, increased glucose levels in the blood and intestine lumen, and exposure of intestinal epithelial (IE) cells to high glucose (HG) concentrations. It has been shown that hyperglycemia promotes cell proliferation, migration, and adhesion in various tumor cell lines [2,24,31,46], including the colon [5,28,35,47]. It is also associated with metastasis and may play a part in reengineering cancer cells in primary lesions. Epithelial barrier function is a key feature of intestinal health [6–8]. Various works have investigated the effect of HG on intestinal barrier properties. However, contradictory results have been described, which can be explained by the different experimental conditions used, in particular concerning exposure time to HG. This exposure time is very frequently short, ranging from 1 to 4 days [24,26,29,31,35,36,46,48–53]. Finally, few studies have evaluated the effect of longer exposure time to HG on the development and characteristics of the intestinal barrier [21,27]. And yet, long-term high glucose exposure is certainly the process that contributes to the development of diseases. For this reason, investigation is warranted to better understand the adaptive physiological changes in IE cells in response to HG consumption, and thus in long-term exposure, as the mechanisms underlying this process remain unclear.

To closely mimic the human intestinal barrier, standard monoculture models with Caco-2 monolayers have been used extensively. However, they form monolayers of enterocyte-like

cells and thus exhibit numerous limitations, such as the lack of mucus layer. Mucus-secreting goblet cells are the second major cell type of the IE and they are frequently represented by HT29-MTX cells. Accordingly, the co-culture of Caco-2 cells with HT29-MTX cells has been referred to as a more predictable experimental cell model than these IE cells in monoculture [12–19].

A normal physiological level of glucose is considered to be 5.5 mM, whereas the glucose concentration in media is frequently 25 mM when investigating the influence of HG on cells [1,21–27]. Surprisingly, this excessive amount of glucose is quite common in experimental settings for the maintenance of Caco-2 and HT29-MTX cells [12,54,55]. Many studies that do not even mention the concentration of glucose in their media frequently used DMEM medium that probably contains HG concentrations [13,14,16–19,42,43,56]. However, this concentration appears to be comparable to the hyperglycemia condition and patients with uncontrolled severe diabetes [1,23].

The present study aimed to explore the impact of these two glucose concentrations (NG and HG) in a long-term exposure condition on various characteristics of IE cells such as proliferation, integrity, permeability, cell morphology, functionality, expression, and localisation of junctional proteins (OCLN, ZO-1 and E-cad). We used *in vitro* models combining Caco-2 and HT29-MTX cells in both monoculture and co-culture. Confocal microscopy demonstrated that growing cells mainly formed a monolayer, especially in NG as at some positions, multilayers appeared in HG. The monolayers were at confluency from 7 days and remained stable for more than 21 days. In both media, we noted the appearance of domes characteristic of Caco-2 cells cultured on plates, indicating correct differentiation of the cells, even on plates compared to insert membranes. As time progressed, the differences in morphology became more pronounced between monolayers grown in HG or NG medium for Caco-2 and HT29-MTX cells, with layers appearing denser and less organized in HG (Fig. 3,

8 and 9). Navabi *et al.* previously found that most cell lines grew faster and in a more disorganized manner with HG content compared to lower glucose content [57]. Béduneau *et al.* revealed the formation of multilayers in an HT29-MTX model and in a Caco-2/HT29-MTX co-culture cultured in HG medium [58]. In addition, Lindner *et al.* have recently shown a time-dependent formation of darker regions in the HT29-MTX monolayer, making it difficult to focus during microscopic imaging [59]. They suggested that HT29-MTX monolayers are capable of expanding three-dimensionally leading to the presence of multi-layered areas, explaining the accumulation of mucus that decreased light transmission in these respective areas [59]. As in NG conditions, HT29-MTX cells have decreased proliferation capability (Fig. 1), these cells are less able to expand three-dimensionally, which is consistent with our morphological result.

TEER measurement is a reliable method for confirming the integrity and permeability of a monolayer. It also makes it possible to characterize the presence of tight junctions between cells. All the monolayers displayed a continuous increase in TEER in the first 18 days after seeding (Fig. 2 and 11D). As previously shown in the literature [14–17,23,37,43,54,56,58,60], HT29-MTX monolayers have very low resistance. Furthermore, TEER values of Caco-2 and HT29-MTX co-culture monolayers decreased as the ratio of Caco-2 cells decreased because these cells form tighter junctions than HT29-MTX cells. Interestingly, HT29-MTX and Caco-2 cells exhibited decreased resistance when cultured in HG medium, further supporting the barrier destabilization induced by HG. Navabi *et al.* previously suggested the negative effect of glucose on the integrity of the monolayer when they detected a decrease in the epithelial resistance of the LS513 cell line grown in the DMEM medium compared to RPMI medium which contains half the amount of glucose [57]. While some studies have also shown a decrease in TEER in the presence of HG [23,36,37,48,52], other studies have observed that there was no effect [21,38]. Villarroel *et al.* even found that human retinal pigment epithelia

cell lines (ARPE-19) showed higher TEER when they were grown in HG medium [27]. This discrepancy may be due to different experimental protocols, but it could also be due to exposure times and cell types, two factors probably crucial in the HG effect. In our study, we highlighted that while the effect of HG in long-term exposure on the permeability of Caco-2 cells was not drastic when the cells were in monoculture, the impact was increasingly significant when they were co-cultured with an increasing proportion of HT29-MTX cells. Similar results were found with apical to basolateral fluxes of FITC-dextran. Caco-2 cells showed very low permeability in both media compared to HT29-MTX cells. FITC-dextran fluxes of Caco-2 and HT29-MTX co-culture monolayers increased as the ratio of Caco-2 cells decreased. Moreover, HG medium slightly but significantly increased the permeability of the co-culture monolayers at 24h, especially as the proportion of HT29-MTX cells increased (Fig. 11E).

The integrity and permeability of the epithelial barrier are accomplished by the formation of complex protein networks that mechanically connect adjacent cells and seal the intercellular space. These protein networks linking epithelial cells form intercellular junctions that include in particular tight junctions (TJ) and adherens junctions (AJ) [6,9,10]. TJ regulate paracellular permeability across epithelial cells, while AJ mediate adhesive contact that supports the mechanical integrity of the epithelial barrier. We studied the most well-known: ZO-1 and OCLN for TJ proteins, and E-cad for an AJ protein.

Although we observed small changes in the mRNA and protein expressions of the junction proteins tested for Caco-2 and HT29-MTX cells in HG medium, we mainly observed low variation, less than 2-fold, which may be not significant (Fig. 6 and 7). Nevertheless, for Caco-2 cells, we found that mRNA and protein expressions of ZO-1, E-cad and OCLN tended to be reduced in HG medium. Results for HT29-MTX cells were more complex, with modification depending on both the protein and time. To go further, we assessed the barrier

integrity through analysis of protein immunofluorescence staining to visualize these cell-cell junctions. Distributions of TJ and AJ proteins were examined with confocal laser scanning microscopy (Fig. 8). As expected, images confirmed the formation of confluent monolayers expressing the junction proteins between neighboring cells at the apical and lateral side of the cells. This typical structural pattern was generally observed for all the proteins of interest in both media. Nevertheless, fluorescence intensities of all junction proteins were greatly reduced in the HG condition compared with the NG condition. For Caco-2 cells and ZO-1, we also found a time-dependent decrease in the intensities and structuring in both media. Concerning HT29-MTX cells, the results are more ambiguous to interpret. We can note that a nonlinear relationship between mRNA and protein expression levels and/or localization of these proteins may be related at some points to post-transcription efficiency and the degradation process. It is noteworthy that most studies investigated the effects of HG after a short time exposure, from 1 to 4 days [24,26,29,31,35,36,46,48–53], in animal intestine tissue [37], in other cell lines from the intestine [22,28,52] or from different organs, such as the breast [28], retina [27], pancreas [46] or endometrium [24]. These studies have found either decreased expression for ZO1 [27,30,36,37,52], OCLN [37,52], E-cad [28,30,35,36,46] or no change for ZO1 [26,48] and OCLN [26,27,36].

Recently, Boztepe and Gulec evaluated the effect of HG on monolayer structure formation and TJ permeability of Caco-2 cells. They also showed that the TEER levels of NG and HG-treated 21-day post-confluent Caco-2 cell groups were not significantly different and that OCLN and ZO1 mRNA levels were also not significantly affected by HG treatment [21]. They concluded that HG did not interfere with barrier formation by monolayer Caco-2 cells. Villarroel *et al*. explored the effect of HG on the expression of TJ proteins (OCLN, ZO-1 and claudin-1) in ARPE-19 cells [27]. They found that OCLN and ZO-1 mRNA and protein levels were similar in cultures maintained in both NG and HG media for 3 weeks. While they did

not see any variation in the immunolocalization of ZO-1, they did not show the result for OCLN.

To the best of our knowledge, this is the first time that confocal microscopy was performed to visualize the structural network of TJ and AJ proteins on both Caco-2 and HT29-MTX cell monolayers cultured in long-term exposure to HG. We confirmed their presence around cell membranes between the neighboring cells forming the well-organized network, known for these intercellular junction proteins. Interestingly, experiments demonstrated that for both cell lines, HG induced a remarkable reduction in the fluorescence intensity of ZO-1, E-cad and OCLN. Moreover, at certain positions, HG triggered a disruption in both monolayer morphology and the particular structure. Transmission electron microscopy experiments could be performed to confirm these morphological alterations. These morphological changes are in accordance with our previous results, showing reduced TEER values and increased FITC-dextran permeability with the cell monolayers maintained in the HG condition. Taken together, these results suggest that HG reduces the physical barrier properties of Caco-2 and HT29-MTX cell monolayers, and probably the IE *in vivo*, by inducing morphological changes to the epithelial barrier, especially through redistribution of epithelial intercellular junction proteins. Consequently, changes in barrier permeability were accompanied by reorganization of TJ and AJ ultrastructures, confirming a link between structural and functional regulation. It has been reported that changes in the density of epithelial junctions and/or distribution pattern can critically contribute to barrier loss and various gastrointestinal disorders [6,7]. Accordingly, the effects of HG on the barrier are not due to drastic changes in the overall protein content but rather to a reorganization of these proteins. Acharya et al. previously showed that the amount of E-cad that concentrated to form an apical zonula adherens can be significantly reduced, without change in the total or surface levels of E-cad [61]. Our results showed a more intense and therefore certainly thicker localization of junction proteins at

lateral cell-cell contact points in NG conditions. The reduction in protein levels detectable at cell junctions under HG conditions highlighted a variation in protein localization in cells, with fewer proteins concentrated at cell junctions. This redistribution suggests a less effective junctional recruitment of proteins, leading to a decrease in protein density at junctions [62]. This reorganization and loss of adhesion between cells induced by HG could also explain how HG significantly enhanced the invasive and migratory capabilities of cells, in particular CRC cells [9,35], which is in line with the results we obtained in this present work (Fig. 5). These features are two characteristics of cancer and play an important role in cancer progression, promoting the growth and metastasis of tumor cells [46]. In addition to the impermeable lining of IE cells, other properties such as the mucus layer are important for maintaining an adequate barrier function. Alcian blue stained cell monolayers allowed us to visualise mucus formation (Fig. 9, 11A and 11B). In both media, as previously shown [14,15,17,42,43,58], mucus release is proportional to increasing amounts of HT29-MTX cells. In our present work, we revealed that this enhancement is more important in the HG medium. Although our experiments on HT29-MTX monolayers in monoculture did not show significant modification in mucus production between the NG or HG media, the same experiments on HT29-MTX monolayers in co-culture with Caco-2 cells finally indicated an increase in staining areas in HG medium. Stress induced by HG may explain this increase. Such stress-induced production of mucins was previously demonstrated for HT29-MTX [59,63]. In addition, HG-induced mucin production has previously been shown in human airway epithelial cells [64]. This increase may be due to accelerated maturation of the HT29-MTX cells towards the goblet cell phenotype, the presence of multicellular layers, and/or activation of the ROS signaling pathway known to increase mucin production [64].

In co-culture, the darker stained blue areas are probably close to the areas of HT29-MTX cell placement, producing the mucus. It was shown that HT29-MTX cells are able to maintain

their intrinsic properties, producing mucus not only when they are in monoculture but also when they are in co-culture [13,17,58]. In these studies, the authors did not precisely indicate the glucose concentration in the DMEM medium. We assume that they used the HG concentration, like most experiments using these epithelial cells. In our study, we revealed that this ability of HT29-MTX cells to maintain high mucus production efficiency while in co-culture with Caco-2 cells is slightly diminished in NG medium. HG may affect the ability of HT29-MTX cells to generate and/or secrete mucus. The lack of an effect that is visible to the eye with cells in monoculture may be due to a saturation of mucus production distributed over the entire support surface. It may also be due to a difference in the composition of the mucus produced by the cells in monoculture or co-culture. Recently, McCright *et al.* showed that the mucus secreted by the co-cultures was more viscoelastic than that secreted by the monoculture of HT29-MTX cells [42].

ALP is a membrane-bound enzyme localized in the brush border of enterocytes in the human IE. Expression of the protein and its activity can thus be used to monitor the differentiation of enterocyte-like cells. While a few methods have been described in the literature [15,17,43,54], there is really no standard technique. In the present study, we developed a fast and reliable method for measuring the ALP activity of the monolayers composed of Caco-2 or HT29-MTX cells in monoculture or co-culture in NG or HG media. We used naphthol AS-MX (N) and fast red TR (FR) as substrates of the ALP enzyme and the ability of the corresponding reaction product (N-FR) to absorb visible light at 525 nm to quantify the activity. Increased absorbance indicated increased of ALP activity. Care should be taken not to use a fixative solution before performing ALP measurement as this step damages the enzyme activity. Previous studies used these substrates, however they used light microscopy to visualize the ALP activity [15,54]. Schimpel *et al.* also described the method using an absorbance microplate reader but the absorbance was measured at 405 nm [43]. Measurements with this

wavelength did not show consistent results, which can be explained by the spectrum of the product. Effectively, while N-FR did exhibit a small shoulder peak at 405 nm, its maximum absorption peaks were located at 525 and 565 nm. No signal was detected with HT29-MTX cells, confirming the absence of ALP activity by these cells. For Caco-2 monolayers, ALP activities increased progressively from day 7 to day 21 (Fig. 10 and 11C). HG tended to slightly decrease the ALP activity of the monolayers, especially in co-culture, but the differences were small and not significant under our experimental conditions, suggesting that HG does not drastically affect enterocyte activity. Our current study supports the hypothesis that the behavior of the cells varies depending on whether they are alone or combined with another cell type, suggesting a cross-relationship between enterocytes and goblet cells. We demonstrated a stronger effect of HG on the different functionalities (TEER, mucus production and ALP activity) of monolayers with Caco-2 and HT29-MTX cells in co-culture than in monoculture.

In the present investigation, *in vitro* models composed of Caco-2 and/or HT29-MTX cells were used. These two cell lines are routinely cultured in the presence of high levels of glucose (25 mM) [12,54,55], since this condition is thought to promote rapid growth and differentiation and to ensure the survival of most cells over long periods of cell culture without the need to control glucose concentration. However, as confirmed by our study, this hyperglycemic condition may lead to changes in cellular processes. Consequently, a particular attention should be brought to the concentration of glucose in culture conditions using *in vitro* models to be closer to physiological conditions, and the results of studies using high glucose concentrations should be interpreted with caution. In the current study, we highlighted that most of the techniques applied to *in vitro* models composed of Caco-2 and/or HT29-MTX cells to characterize the morphology and functionality of the intestinal barrier can be performed in the presence of physiological glucose concentration. Furthermore, we provide

evidence that long-term exposure to high glucose levels impairs various barrier characteristics and functions, suggesting that diet can play a role in the health of the gut barrier. Even though high intestinal luminal glucose levels, caused by high dietary glucose consumption or pathology such as hyperglycemia or diabetes, only slightly alter the properties of the intestinal barrier, these long-term alterations can cause life-threatening complications and have important pathophysiological consequences. In addition, they are sufficient to weaken the intestinal barrier and make it sensitive to any other foreign attack (microbes, xenobiotics...). The mechanisms underlying glucose fluctuation and intestinal barrier dysfunction involve morphological and structural alteration of IE cells and of the monolayer they constitute. We cannot rule out other pathways being involved in these mechanisms. It is worth noting that during cell growth in HG medium, particularly with HT29-MTX cells, the medium changed color slightly to yellow after three days of culture, indicating that the pH was altered. High glucose probably enhanced various cellular metabolisms increasing metabolites released by the cells. These metabolites could be one of the mechanisms involved in the effect of high glucose on cells. It has been shown that epithelial barrier dysfunction may result from focal disruptions of tight junctional proteins or from the contraction of actin and myosin II bands, which constitute the perijunctional actomyosin ring [65]. In addition, Borghi *et al*. revealed a constitutive function of E-cad as a link between the cell membrane and the actomyosin cytoskeleton [66]. Myosin contraction acts on attached F-actin, which is bound to junction proteins, resulting in increased epithelial paracellular permeability. Even if we did not observe a significant impact of HG on the F-actin arrangement (data not shown), we cannot exclude an effect of HG on myosin II activity and on the contraction of the perijunctional actomyosin ring. Further studies are needed to clarify this question. The mechanisms by which high glucose concentrations compromise intestinal epithelial cell function *in vivo* may also involve interconnected processes as varied as they are complex, including insulin production

[2,8,25,28,30,44] or the microbiota [8,30,44,45]. Besides intestinal barrier dysfunction, the long-term HG exposure condition of our experiments has enabled us to identify differences in the evolution of cell densities in monolayers for both Caco-2 and HT29-MTX cells. It is conceivable that under pathological conditions, high glucose concentration has an impact on intestinal epithelial renewal. The impaired intestinal barrier can be a catalyst for the development of various diseases. In addition, deregulation of glucose homeostasis may affect treatment efficacy in certain patients [31,47,67]. It has been shown that supraphysiologic glucose reduces the effectiveness of metformin in various molecular subtypes of cancer cells, but may be overcome by using higher doses of metformin [31]. Ma *et al*. showed that, compared to physiological NG concentrations, HG leads to increased GI50 of 5-FU in four colon cancer cell lines [47]. Controlling hyperglycemia remains a major therapeutical method for reducing damage to IE cells and the barrier, and for improving therapy [5,8,22,25,52]. Consequently, new therapeutic strategies to manipulate the intestinal barrier and repair its functions have been tested clinically and in various diseases, repairing intestinal barrier dysfunction in many cases [6–8]. These strategies may include diet, but also drugs, probiotics, or natural products.

REFERENCES

1. Clement, S.; Braithwaite, S.S.; Magee, M.F.; Ahmann, A.; Smith, E.P.; Schafer, R.G.; Hirsch, I.B.; American Diabetes Association Diabetes in Hospitals Writing Committee Management of Diabetes and Hyperglycemia in Hospitals. *Diabetes Care* **2004**, *27*, 553–591, doi:10.2337/diacare.27.2.553.
2. Giri, B.; Dey, S.; Das, T.; Sarkar, M.; Banerjee, J.; Dash, S.K. Chronic Hyperglycemia Mediated Physiological Alteration and Metabolic Distortion Leads to Organ Dysfunction, Infection, Cancer Progression and Other Pathophysiological Consequences: An Update on Glucose Toxicity. *Biomed Pharmacother* **2018**, *107*, 306–328, doi:10.1016/j.biopha.2018.07.157.
3. Hruby, A.; Hu, F.B. The Epidemiology of Obesity: A Big Picture. *Pharmacoeconomics* **2015**, *33*, 673–689, doi:10.1007/s40273-014-0243-x.
4. World Health Organization. Regional Office for Europe *WHO European Regional Obesity Report 2022*; World Health Organization. Regional Office for Europe, 2022; ISBN 978-92-890-5773-8.
5. Duan, W.; Shen, X.; Lei, J.; Xu, Q.; Yu, Y.; Li, R.; Wu, E.; Ma, Q. Hyperglycemia, a Neglected Factor during Cancer Progression. *Biomed Res Int* **2014**, *2014*, 461917, doi:10.1155/2014/461917.
6. Groschwitz, K.R.; Hogan, S.P. Intestinal Barrier Function: Molecular Regulation and Disease Pathogenesis. *J Allergy Clin Immunol* **2009**, *124*, 3–20; quiz 21–22, doi:10.1016/j.jaci.2009.05.038.
7. Odenwald, M.A.; Turner, J.R. The Intestinal Epithelial Barrier: A Therapeutic Target? *Nat Rev Gastroenterol Hepatol* **2017**, *14*, 9–21, doi:10.1038/nrgastro.2016.169.
8. Zhang, Y.; Zhu, X.; Yu, X.; Novák, P.; Gui, Q.; Yin, K. Enhancing Intestinal Barrier Efficiency: A Novel Metabolic Diseases Therapy. *Front Nutr* **2023**, *10*, 1120168, doi:10.3389/fnut.2023.1120168.
9. Bhat, A.A.; Uppada, S.; Achkar, I.W.; Hashem, S.; Yadav, S.K.; Shanmugakonar, M.; Al-Naemi, H.A.; Haris, M.; Uddin, S. Tight Junction Proteins and Signaling Pathways in Cancer and Inflammation: A Functional Crosstalk. *Front Physiol* **2018**, *9*, 1942, doi:10.3389/fphys.2018.01942.
10. Niessen, C.M. Tight Junctions/Adherens Junctions: Basic Structure and Function. *J Invest Dermatol* **2007**, *127*, 2525–2532, doi:10.1038/sj.jid.5700865.
11. Estaki, M.; DeCoffe, D.; Gibson, D.L. Interplay between Intestinal Alkaline Phosphatase, Diet, Gut Microbes and Immunity. *World J Gastroenterol* **2014**, *20*, 15650–15656, doi:10.3748/wjg.v20.i42.15650.
12. Akbari, A.; Lavasanifar, A.; Wu, J. Interaction of Cruciferin-Based Nanoparticles with Caco-2 Cells and Caco-2/HT29-MTX Co-Cultures. *Acta Biomater* **2017**, *64*, 249–258, doi:10.1016/j.actbio.2017.10.017.
13. Araújo, F.; Sarmento, B. Towards the Characterization of an in Vitro Triple Co-Culture Intestine Cell Model for Permeability Studies. *Int J Pharm* **2013**, *458*, 128–134, doi:10.1016/j.ijpharm.2013.10.003.
14. Boegh, M.; Baldursdóttir, S.G.; Müllertz, A.; Nielsen, H.M. Property Profiling of Biosimilar Mucus in a Novel Mucus-Containing in Vitro Model for Assessment of Intestinal Drug Absorption. *Eur J Pharm Biopharm* **2014**, *87*, 227–235, doi:10.1016/j.ejpb.2014.01.001.
15. Chen, X.-M.; Elisia, I.; Kitts, D.D. Defining Conditions for the Co-Culture of Caco-2 and HT29-MTX Cells Using Taguchi Design. *J Pharmacol Toxicol Methods* **2010**, *61*, 334–342, doi:10.1016/j.vascn.2010.02.004.
16. Lehner, R.; Wohlleben, W.; Septiadi, D.; Landsiedel, R.; Petri-Fink, A.; Rothen-Rutishauser, B. A Novel 3D Intestine Barrier Model to Study the Immune Response upon Exposure to Microplastics. *Arch Toxicol* **2020**, *94*, 2463–2479, doi:10.1007/s00204-020-02750-1.
17. Pan, F.; Han, L.; Zhang, Y.; Yu, Y.; Liu, J. Optimization of Caco-2 and HT29 Co-Culture in Vitro Cell Models for Permeability Studies. *Int J Food Sci Nutr* **2015**, *66*, 680–685, doi:10.3109/09637486.2015.1077792.

18. Pham, V.T.; Fehlbaum, S.; Seifert, N.; Richard, N.; Bruins, M.J.; Sybesma, W.; Rehman, A.; Steinert, R.E. Effects of Colon-Targeted Vitamins on the Composition and Metabolic Activity of the Human Gut Microbiome- a Pilot Study. *Gut Microbes* **2021**, *13*, 1–20, doi:10.1080/19490976.2021.1875774.

19. Pham, V.T.; Seifert, N.; Richard, N.; Raederstorff, D.; Steinert, R.E.; Prudence, K.; Mohajeri, M.H. The Effects of Fermentation Products of Prebiotic Fibres on Gut Barrier and Immune Functions in Vitro. *PeerJ* **2018**, *6*, e5288, doi:10.7717/peerj.5288.

20. Quagliaro, L.; Piconi, L.; Assaloni, R.; Martinelli, L.; Motz, E.; Ceriello, A. Intermittent High Glucose Enhances Apoptosis Related to Oxidative Stress in Human Umbilical Vein Endothelial Cells: The Role of Protein Kinase C and NAD(P)H-Oxidase Activation. *Diabetes* **2003**, *52*, 2795–2804, doi:10.2337/diabetes.52.11.2795.

21. Boztepe, T.; Gulec, S. Investigation of the Influence of High Glucose on Molecular and Genetic Responses: An in Vitro Study Using a Human Intestine Model. *Genes Nutr* **2018**, *13*, 11, doi:10.1186/s12263-018-0602-x.

22. Chen, B.; Jia, Y.; Lu, D.; Sun, Z. Acute Glucose Fluctuation Promotes in Vitro Intestinal Epithelial Cell Apoptosis and Inflammation via the NOX4/ROS/JAK/STAT3 Signaling Pathway. *Exp Ther Med* **2021**, *22*, 688, doi:10.3892/etm.2021.10120.

23. D'Souza, V.M.; Shertzer, H.G.; Menon, A.G.; Pauletti, G.M. High Glucose Concentration in Isotonic Media Alters Caco-2 Cell Permeability. *AAPS PharmSci* **2003**, *5*, E24, doi:10.1208/ps050324.

24. Han, J.; Zhang, L.; Guo, H.; Wysham, W.Z.; Roque, D.R.; Willson, A.K.; Sheng, X.; Zhou, C.; Bae-Jump, V.L. Glucose Promotes Cell Proliferation, Glucose Uptake and Invasion in Endometrial Cancer Cells via AMPK/MTOR/S6 and MAPK Signaling. *Gynecol Oncol* **2015**, *138*, 668–675, doi:10.1016/j.ygyno.2015.06.036.

25. Leontieva, O.V.; Demidenko, Z.N.; Blagosklonny, M.V. Rapamycin Reverses Insulin Resistance (IR) in High-Glucose Medium without Causing IR in Normoglycemic Medium. *Cell Death Dis* **2014**, *5*, e1214, doi:10.1038/cddis.2014.178.

26. Pereira, M.T.; Malik, M.; Nostro, J.A.; Mahler, G.J.; Musselman, L.P. Effect of Dietary Additives on Intestinal Permeability in Both Drosophila and a Human Cell Co-Culture. *Dis Model Mech* **2018**, *11*, dmm034520, doi:10.1242/dmm.034520.

27. Villarroel, M.; García-Ramírez, M.; Corraliza, L.; Hernández, C.; Simó, R. Effects of High Glucose Concentration on the Barrier Function and the Expression of Tight Junction Proteins in Human Retinal Pigment Epithelial Cells. *Exp Eye Res* **2009**, *89*, 913–920, doi:10.1016/j.exer.2009.07.017.

28. Masur, K.; Vetter, C.; Hinz, A.; Tomas, N.; Henrich, H.; Niggemann, B.; Zänker, K.S. Diabetogenic Glucose and Insulin Concentrations Modulate Transcriptome and Protein Levels Involved in Tumour Cell Migration, Adhesion and Proliferation. *Br J Cancer* **2011**, *104*, 345–352, doi:10.1038/sj.bjc.6606050.

29. Skibbe, K.; Brethack, A.-K.; Sünderhauf, A.; Ragab, M.; Raschdorf, A.; Hicken, M.; Schlichting, H.; Preira, J.; Brandt, J.; Castven, D.; et al. Colorectal Cancer Progression Is Potently Reduced by a Glucose-Free, High-Protein Diet: Comparison to Anti-EGFR Therapy. *Cancers (Basel)* **2021**, *13*, 5817, doi:10.3390/cancers13225817.

30. Thaiss, C.A.; Levy, M.; Grosheva, I.; Zheng, D.; Soffer, E.; Blacher, E.; Braverman, S.; Tengeler, A.C.; Barak, O.; Elazar, M.; et al. Hyperglycemia Drives Intestinal Barrier Dysfunction and Risk for Enteric Infection. *Science* **2018**, *359*, 1376–1383, doi:10.1126/science.aar3318.

31. Wahdan-Alaswad, R.; Fan, Z.; Edgerton, S.M.; Liu, B.; Deng, X.-S.; Arnadottir, S.S.; Richer, J.K.; Anderson, S.M.; Thor, A.D. Glucose Promotes Breast Cancer Aggression and Reduces Metformin Efficacy. *Cell Cycle* **2013**, *12*, 3759–3769, doi:10.4161/cc.26641.

32. Morresi, C.; Cianfruglia, L.; Sartini, D.; Cecati, M.; Fumarola, S.; Emanuelli, M.; Armeni, T.; Ferretti, G.; Bacchetti, T. Effect of High Glucose-Induced Oxidative Stress on Paraoxonase 2 Expression and Activity in Caco-2 Cells. *Cells* **2019**, *8*, 1616, doi:10.3390/cells8121616.

33. Mroueh, F.M.; Noureldein, M.; Zeidan, Y.H.; Boutary, S.; Irani, S.A.M.; Eid, S.; Haddad, M.; Barakat, R.; Harb, F.; Costantine, J.; et al. Unmasking the Interplay between MTOR and Nox4: Novel Insights into the Mechanism Connecting Diabetes and Cancer. *FASEB J* **2019**, *33*, 14051–14066, doi:10.1096/fj.201900396RR.

34. Yang, I.-P.; Miao, Z.-F.; Huang, C.-W.; Tsai, H.-L.; Yeh, Y.-S.; Su, W.-C.; Chang, T.-K.; Chang, S.-F.; Wang, J.-Y. High Blood Sugar Levels but Not Diabetes Mellitus Significantly Enhance Oxaliplatin Chemoresistance in Patients with Stage III Colorectal Cancer Receiving Adjuvant FOLFOX6 Chemotherapy. *Ther Adv Med Oncol* **2019**, *11*, 1758835919866964, doi:10.1177/1758835919866964.

35. Wu, J.; Chen, J.; Xi, Y.; Wang, F.; Sha, H.; Luo, L.; Zhu, Y.; Hong, X.; Bu, S. High Glucose Induces Epithelial-Mesenchymal Transition and Results in the Migration and Invasion of Colorectal Cancer Cells. *Exp Ther Med* **2018**, *16*, 222–230, doi:10.3892/etm.2018.6189.

36. Sharma, S.; Tripathi, P.; Sharma, J.; Dixit, A. Flavonoids Modulate Tight Junction Barrier Functions in Hyperglycemic Human Intestinal Caco-2 Cells. *Nutrition* **2020**, *78*, 110792, doi:10.1016/j.nut.2020.110792.

37. Min, X.-H.; Yu, T.; Qing, Q.; Yuan, Y.-H.; Zhong, W.; Chen, G.-C.; Zhao, L.-N.; Deng, N.; Zhang, L.-F.; Chen, Q.-K. Abnormal Differentiation of Intestinal Epithelium and Intestinal Barrier Dysfunction in Diabetic Mice Associated with Depressed Notch/NICD Transduction in Notch/Hes1 Signal Pathway. *Cell Biol Int* **2014**, *38*, 1194–1204, doi:10.1002/cbin.10323.

38. Dutton, J.S.; Hinman, S.S.; Kim, R.; Attayek, P.J.; Maurer, M.; Sims, C.S.; Allbritton, N.L. Hyperglycemia Minimally Alters Primary Self-Renewing Human Colonic Epithelial Cells While TNFα-Promotes Severe Intestinal Epithelial Dysfunction. *Integr Biol (Camb)* **2021**, *13*, 139–152, doi:10.1093/intbio/zyab008.

39. Lerkdumnernkit, N.; Sricharoenvej, S.; Lanlua, P.; Niyomchan, A.; Baimai, S.; Chookliang, A.; Plaengrit, K.; Pianrumluk, S.; Manoonpol, C. The Effects of Early Diabetes on Duodenal Alterations in the Rats. *International Journal of Morphology* **2022**, *40*, 389–395, doi:10.4067/S0717-95022022000200389.

40. Volynets, V.; Louis, S.; Pretz, D.; Lang, L.; Ostaff, M.J.; Wehkamp, J.; Bischoff, S.C. Intestinal Barrier Function and the Gut Microbiome Are Differentially Affected in Mice Fed a Western-Style Diet or Drinking Water Supplemented with Fructose. *J Nutr* **2017**, *147*, 770–780, doi:10.3945/jn.116.242859.

41. Grasset, E.; Pinto, M.; Dussaulx, E.; Zweibaum, A.; Desjeux, J.F. Epithelial Properties of Human Colonic Carcinoma Cell Line Caco-2: Electrical Parameters. *Am J Physiol* **1984**, *247*, C260-267, doi:10.1152/ajpcell.1984.247.3.C260.

42. McCright, J.; Sinha, A.; Maisel, K. Generating an In Vitro Gut Model with Physiologically Relevant Biophysical Mucus Properties. *Cell Mol Bioeng* **2022**, *15*, 479–491, doi:10.1007/s12195-022-00740-0.

43. Schimpel, C.; Teubl, B.; Absenger, M.; Meindl, C.; Fröhlich, E.; Leitinger, G.; Zimmer, A.; Roblegg, E. Development of an Advanced Intestinal in Vitro Triple Culture Permeability Model to Study Transport of Nanoparticles. *Mol Pharm* **2014**, *11*, 808–818, doi:10.1021/mp400507g.

44. Lustig, R.H.; Collier, D.; Kassotis, C.; Roepke, T.A.; Kim, M.J.; Blanc, E.; Barouki, R.; Bansal, A.; Cave, M.C.; Chatterjee, S.; et al. Obesity I: Overview and Molecular and Biochemical Mechanisms. *Biochemical Pharmacology* **2022**, *199*, 115012, doi:10.1016/j.bcp.2022.115012.

45. Yao, Q.; Yu, Z.; Meng, Q.; Chen, J.; Liu, Y.; Song, W.; Ren, X.; Zhou, J.; Chen, X. The Role of Small Intestinal Bacterial Overgrowth in Obesity and Its Related Diseases. *Biochemical Pharmacology* **2023**, *212*, 115546, doi:10.1016/j.bcp.2023.115546.

46. Han, L.; Peng, B.; Ma, Q.; Ma, J.; Li, J.; Li, W.; Duan, W.; Chen, C.; Liu, J.; Xu, Q.; et al. Indometacin Ameliorates High Glucose-Induced Proliferation and Invasion via Modulation of e-Cadherin in Pancreatic Cancer Cells. *Curr Med Chem* **2013**, *20*, 4142–4152, doi:10.2174/09298673113209990249.

47. Ma, Y.-S.; Yang, I.-P.; Tsai, H.-L.; Huang, C.-W.; Juo, S.-H.H.; Wang, J.-Y. High Glucose Modulates Antiproliferative Effect and Cytotoxicity of 5-Fluorouracil in Human Colon Cancer Cells. *DNA Cell Biol* **2014**, *33*, 64–72, doi:10.1089/dna.2013.2161.

48. Alfuraih, S.; Barbarino, A.; Ross, C.; Shamloo, K.; Jhanji, V.; Zhang, M.; Sharma, A. Effect of High Glucose on Ocular Surface Epithelial Cell Barrier and Tight Junction Proteins. *Invest Ophthalmol Vis Sci* **2020**, *61*, 3, doi:10.1167/iovs.61.11.3.

49. Cheng, Y.-C.; Chu, L.-W.; Chen, J.-Y.; Hsieh, S.-L.; Chang, Y.-C.; Dai, Z.-K.; Wu, B.-N. Loganin Attenuates High Glucose-Induced Schwann Cells Pyroptosis by Inhibiting ROS Generation and NLRP3 Inflammasome Activation. *Cells* **2020**, *9*, 1948, doi:10.3390/cells9091948.

50. Filippello, A.; Di Mauro, S.; Scamporrino, A.; Malaguarnera, R.; Torrisi, S.A.; Leggio, G.M.; Di Pino, A.; Scicali, R.; Purrello, F.; Piro, S. High Glucose Exposure Impairs L-Cell Differentiation in Intestinal Organoids: Molecular Mechanisms and Clinical Implications. *Int J Mol Sci* **2021**, *22*, 6660, doi:10.3390/ijms22136660.

51. Gan, J.; Huang, M.; Lan, G.; Liu, L.; Xu, F. High Glucose Induces the Loss of Retinal Pericytes Partly via NLRP3-Caspase-1-GSDMD-Mediated Pyroptosis. *Biomed Res Int* **2020**, *2020*, 4510628, doi:10.1155/2020/4510628.

52. Qing, Q.; Zhang, S.; Chen, Y.; Li, R.; Mao, H.; Chen, Q. High Glucose-Induced Intestinal Epithelial Barrier Damage Is Aggravated by Syndecan-1 Destruction and Heparanase Overexpression. *J Cell Mol Med* **2015**, *19*, 1366–1374, doi:10.1111/jcmm.12523.

53. Suarez, S.; McCollum, G.W.; Jayagopal, A.; Penn, J.S. High Glucose-Induced Retinal Pericyte Apoptosis Depends on Association of GAPDH and Siah1. *J Biol Chem* **2015**, *290*, 28311–28320, doi:10.1074/jbc.M115.682385.

54. Nollevaux, G.; Devillé, C.; El Moualij, B.; Zorzi, W.; Deloyer, P.; Schneider, Y.-J.; Peulen, O.; Dandrifosse, G. Development of a Serum-Free Co-Culture of Human Intestinal Epithelium Cell-Lines (Caco-2/HT29-5M21). *BMC Cell Biol* **2006**, *7*, 20, doi:10.1186/1471-2121-7-20.

55. Talbot, P.; Radziwill-Bienkowska, J.M.; Kamphuis, J.B.J.; Steenkeste, K.; Bettini, S.; Robert, V.; Noordine, M.-L.; Mayeur, C.; Gaultier, E.; Langella, P.; et al. Food-Grade TiO2 Is Trapped by Intestinal Mucus in Vitro but Does Not Impair Mucin O-Glycosylation and Short-Chain Fatty Acid Synthesis in Vivo: Implications for Gut Barrier Protection. *J Nanobiotechnology* **2018**, *16*, 53, doi:10.1186/s12951-018-0379-5.

56. Pontier, C.; Pachot, J.; Botham, R.; Lenfant, B.; Arnaud, P. HT29-MTX and Caco-2/TC7 Monolayers as Predictive Models for Human Intestinal Absorption: Role of the Mucus Layer. *J Pharm Sci* **2001**, *90*, 1608–1619, doi:10.1002/jps.1111.

57. Navabi, N.; McGuckin, M.A.; Lindén, S.K. Gastrointestinal Cell Lines Form Polarized Epithelia with an Adherent Mucus Layer When Cultured in Semi-Wet Interfaces with Mechanical Stimulation. *PLoS One* **2013**, *8*, e68761, doi:10.1371/journal.pone.0068761.

58. Béduneau, A.; Tempesta, C.; Fimbel, S.; Pellequer, Y.; Jannin, V.; Demarne, F.; Lamprecht, A. A Tunable Caco-2/HT29-MTX Co-Culture Model Mimicking Variable Permeabilities of the Human Intestine Obtained by an Original Seeding Procedure. *Eur J Pharm Biopharm* **2014**, *87*, 290–298, doi:10.1016/j.ejpb.2014.03.017.

59. Lindner, M.; Laporte, A.; Block, S.; Elomaa, L.; Weinhart, M. Physiological Shear Stress Enhances Differentiation, Mucus-Formation and Structural 3D Organization of Intestinal Epithelial Cells In Vitro. *Cells* **2021**, *10*, 2062, doi:10.3390/cells10082062.

60. Gagnon, M.; Zihler Berner, A.; Chervet, N.; Chassard, C.; Lacroix, C. Comparison of the Caco-2, HT-29 and the Mucus-Secreting HT29-MTX Intestinal Cell Models to Investigate Salmonella Adhesion and Invasion. *J. Microbiol. Methods* **2013**, *94*, 274–279, doi:10.1016/j.mimet.2013.06.027.

61. Acharya, B.R.; Wu, S.K.; Lieu, Z.Z.; Parton, R.G.; Grill, S.W.; Bershadsky, A.D.; Gomez, G.A.; Yap, A.S. Mammalian Diaphanous 1 Mediates a Pathway for E-Cadherin to Stabilize Epithelial Barriers through Junctional Contractility. *Cell Rep* **2017**, *18*, 2854–2867, doi:10.1016/j.celrep.2017.02.078.

62. Kale, G.R.; Yang, X.; Philippe, J.-M.; Mani, M.; Lenne, P.-F.; Lecuit, T. Distinct Contributions of Tensile and Shear Stress on E-Cadherin Levels during Morphogenesis. *Nat Commun* **2018**, *9*, 5021, doi:10.1038/s41467-018-07448-8.

63. Elzinga, J.; van der Lugt, B.; Belzer, C.; Steegenga, W.T. Characterization of Increased Mucus Production of HT29-MTX-E12 Cells Grown under Semi-Wet Interface with Mechanical Stimulation. *PLoS One* **2021**, *16*, e0261191, doi:10.1371/journal.pone.0261191.

64. Yu, H.; Yang, J.; Xiao, Q.; Lü, Y.; Zhou, X.; Xia, L.; Nie, D. Regulation of High Glucose-Mediated Mucin Expression by Matrix Metalloproteinase-9 in Human Airway Epithelial Cells. *Exp Cell Res* **2015**, *333*, 127–135, doi:10.1016/j.yexcr.2015.02.007.

65. Rodgers, L.S.; Fanning, A.S. Regulation of Epithelial Permeability by the Actin Cytoskeleton. *Cytoskeleton (Hoboken)* **2011**, *68*, 653–660, doi:10.1002/cm.20547.

66. Borghi, N.; Sorokina, M.; Shcherbakova, O.G.; Weis, W.I.; Pruitt, B.L.; Nelson, W.J.; Dunn, A.R. E-Cadherin Is under Constitutive Actomyosin-Generated Tension That Is Increased at Cell-Cell Contacts upon Externally Applied Stretch. *Proc Natl Acad Sci U S A* **2012**, *109*, 12568–12573, doi:10.1073/pnas.1204390109.

67. Zhang, L.; Xu, P.; Cheng, Y.; Wang, P.; Ma, X.; Liu, M.; Wang, X.; Xu, F. Diet-Induced Obese Alters the Expression and Function of Hepatic Drug-Metabolizing Enzymes and Transporters in Rats. *Biochem Pharmacol* **2019**, *164*, 368–376, doi:10.1016/j.bcp.2019.05.002.

AUTHOR CONTRIBUTIONS

Conceptualization, ARC; Methodology, ND, JMG and ARC; Formal analysis; Investigation; Validation, ND, ARC; Funding acquisition, DH and ARC; Writing - original draft ARC; Writing - review & editing, ND, JMG, DH, ARC.

CONFLICT OF INTEREST

The authors declare no conflict of interest.

FIGURE LEGENDS

Table 1. Oligonucleotide sequences of primers used for mRNA quantification using qPCR analysis

Fig. 1. Effect of HG on intestinal cell growth of Caco-2 (A) and HT29-MTX (B) cells. Caco-2 and HT29-MTX cells were grown for 14 days in NG or HG medium. Manual cell counts were carried out on days 3, 5, 7, 10, 12 and 14 after seeding. Results for cell count per well are expressed as mean ± SD of n=4 experiments (two-way ANOVA, **$p < 0.01$, ****$p < 0.0001$ versus NG condition).

Fig. 2. Effect of HG on the TEER (A) and the permeability (B and C) of the intestinal cell monolayer of Caco-2 (A and B) and HT29-MTX cells (A and C). Caco-2 and HT29-MTX cells were seeded at densities of 50 000 cells per well in NG or HG medium. (A) TEER values of the cell monolayer were measured as a function of culture time after seeding in Transwell membranes for 21 days. (B and C) FITC-dextran permeability assay was performed in Transwell membranes at 18 days. FITC-dextran (1 mg/mL in NG or HG medium) was added to the apical chambers and samples were collected from the basolateral chambers at 2h, 4h, 6h and 24h. All data were reported as mean ± SD of n=3-6 experiments (two-way ANOVA, *$p < 0.05$ versus NG condition).

Fig. 3. Effect of HG on the intestinal cell monolayer morphology of Caco-2 (A) and HT29-MTX (B) cells. Representative brightfield images at day 7, day 14 and day 21 of Caco-2 and HT29-MTX cells cultured in NG or HG medium in 96-well plates. Cells grew in confluent monolayers and differentiated over the days of culture. Domes and black spots are indicated with yellow and blue arrows respectively. Cells were photographed with the Operetta CLS™ high throughput microplate imager (5X magnification). Scale bar: 500 µm.

Fig. 4. Effect of HG on the nuclear cell morphology of Caco-2 (A) and HT29-MTX (B) cells. Cells were grown in 96-well plates in NG or HG medium for 7 and 21 days. DNA was

stained with DAPI to reveal the position and morphology of the nuclei. Fluorescence microscopy images were captured with the Operetta CLS™ high throughput microplate imager (63X magnification). Then, fluorescence intensity, area and number of nuclei were measured per well with ImageJ software. Results are expressed as mean ± SD of n=9-10 experiments (two-way ANOVA, *p < 0.05, **p < 0.01, ***p < 0.001 and ****p < 0.0001 versus NG condition).

Fig. 5. Effect of HG on the migration ability of Caco-2 (A and C) and HT29-MTX (B and C) cells. Confluent monolayers of Caco-2 or HT29-MTX cells grown in 12-well plates in NG or HG medium were wounded with a micropipette tip and incubated for 96h. (A and B) Representative brightfield images of scratched areas at 0, 24, 48 and 72h from the scrape, captured by the Operetta CLS™ high throughput microplate imager (5X magnification) to check for wound closure. Scale bar: 500 µm. (C) Cell migration distances covered in mm compared to time zero after scratch formation were measured using ImageJ software. Results are expressed as mean ± SD of n=6 experiments (two-way ANOVA, *p < 0.05, **p < 0.01 and ****p < 0.001 versus NG condition).

Fig. 6. Effect of HG on mRNA expression of junction proteins in Caco-2 (A) and HT29-MTX (B) cells. Total RNA of Caco-2 or HT29-MTX cells grown in 6-well plates in NG or HG medium were extracted at days 7, 14 and 21. The mRNA expressions of ZO-1, OCLN and E-cad were estimated with RT-qPCR. The expression of each target gene was quantified using actin as a normalization control. Expression levels were represented relative to the one in NG medium at day 2 for each protein and the cell lines. Results are expressed as mean ± SD of three independent experiments (two-way ANOVA, *p < 0.05, ***p < 0.001 and ****p < 0.0001 versus NG condition).

Fig. 7. Effect of HG on the protein expression of junction proteins in Caco-2 (A and C) and HT29-MTX (B and D) cells. Total protein contents of Caco-2 or HT29-MTX cells

grown in 6-well plates in NG or HG medium were extracted at days 7, 14 and 21. Levels of ZO-1, OCLN and E-cad were estimated using Western blot. (A and B) Representative images of immunoblots from at least three replicates are shown. β-actin was used as the protein loading control. (C and D) The expression of each target was quantified using densitometry and actin as a normalization control. Results are expressed as mean ± SD of at least three independent experiments (two-way ANOVA, $*p < 0.05$, $**p < 0.01$, $***p < 0.001$ and $****p < 0.0001$ versus NG condition).

Fig. 8. Effect of HG on the structuration of junction proteins in Caco-2 (A and C) and HT29-MTX (B and D) cells. Cells were grown in 96-well plates in NG or HG medium for 7, 14 and 21 days. (A and B) Representative fluorescence microscopy images captured by the Operetta CLS™ high throughput microplate imager (63X magnification). Tight and adherens junction proteins ZO-1, OCLN and E-cad are stained in green. Scale bar: 50 µm. (C and D) z-stack images were generated to show the localization of the proteins in the X-Z planes at day 21. Scale bar: 20 µm.

Fig. 9. Staining of acidic mucins with Alcian blue in Caco-2 and HT29-MTX cell monoculture. Cells were cultured on Transwell membranes for 21 days in NH or HG medium. After Carnoy fixation to preserve the mucus layer, cells were stained with Alcian blue. (A) Representative images captured using Nikon Eclipse Ni-U Upright microscope (2X magnification). Scale bar: 1 mm. (B) Percentage area of Alcian blue positive staining and mean intensity of all blue pixels analyzed using ImageJ software. Results are expressed as mean ± SD of at least three independent experiments. (C) Cells were then paraffin embedded, sectioned, and stained with hematoxylin and eosin. Representative images of cross sections captured using a Hamamatsu NanoZoomer S60 slide scanner (20X magnification) are shown. Scale bar: 50 µm.

Fig. 10. Alkaline phosphatase activity of Caco-2 and HT29-MTX cell monolayers in monoculture. Cells were grown in 96-well plates in NG or HG medium for 7, 14 and 21 days. At the corresponding time, enzymatic reactions were performed for 30 min at 37°C by adding the two substrates, N and FR. The absorbance of the reaction product N-FR was measured at 525 nm. Results are expressed as mean ± SD of at least three independent experiments.

Fig. 11. Effect of HG on the barrier functions of Caco-2 and HT29-MTX monolayers in co-culture at three different seeding cell ratios (9:1, 8:2 and 7:3). (A) and (B) Cells were cultured on Transwell membranes for 21 days in NH or HG medium. After Carnoy fixation to preserve the mucus layer, cells were stained with Alcian blue. (A) Representative images captured using a Nikon Eclipse Ni-U Upright microscope (2X magnification). Scale bar: 1 mm. (B) Percentage area of Alcian blue positive staining and mean intensity of all blue pixels analyzed using ImageJ software. Results are expressed as mean ± SD of at least three independent experiments. (C) Cells were grown in 96-well plates in NG or HG medium for 7, 14 and 21 days. At the corresponding time, enzymatic reactions were performed for 30 min at 37°C by adding the two substrates, N and FR. The absorbance of the reaction product N-FR was measured at 525 nm. Values for HT29-MTX cells, close to the background noise level, were considered as zero. Results are expressed as mean ± SD of at least three independent experiments. (D) Cells were cultured on Transwell membranes for 18 days in NH or HG medium. TEER results are expressed as mean ± SD of n=4-6 independent experiments. (E) FITC-dextran permeability assay was performed in Transwell membranes at 18 days. FITC-dextran (1 mg/mL in NG or HG medium) was added to the apical chambers and samples were collected from the basolateral chambers at 24h. Results are expressed as mean ± SD of n=3 experiments. Statistical analyses were performed using two-way ANOVA (*p < 0.05, **p < 0.01, ***p < 0.001 and ****p < 0.0001 versus NG condition).

Table 1

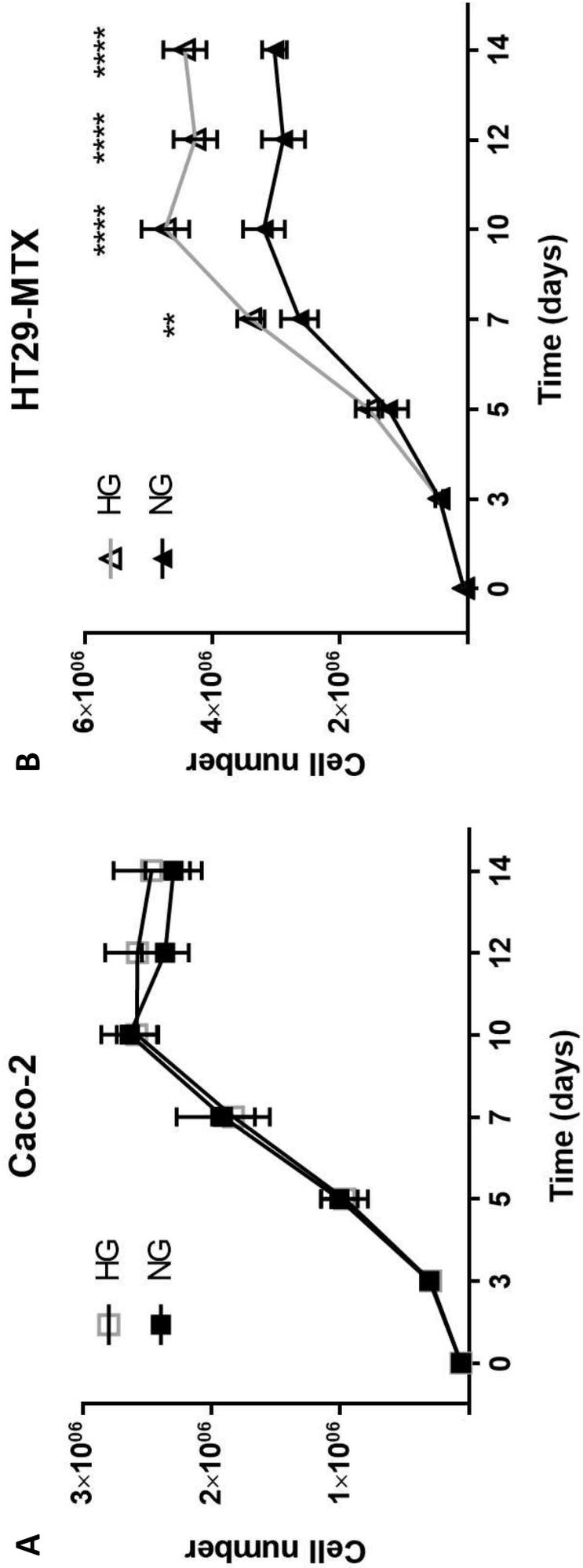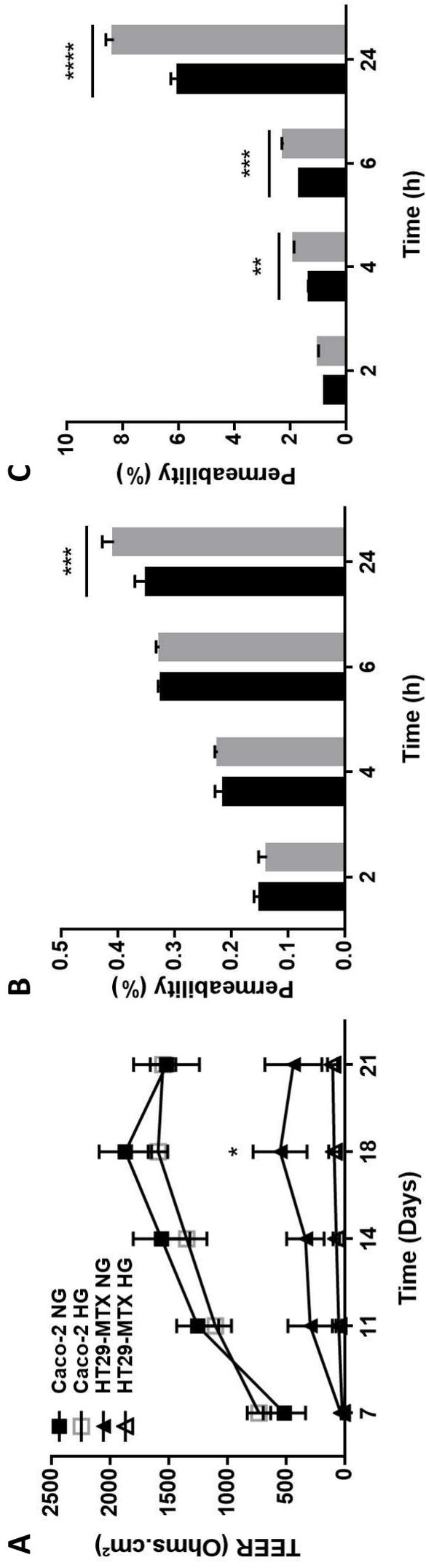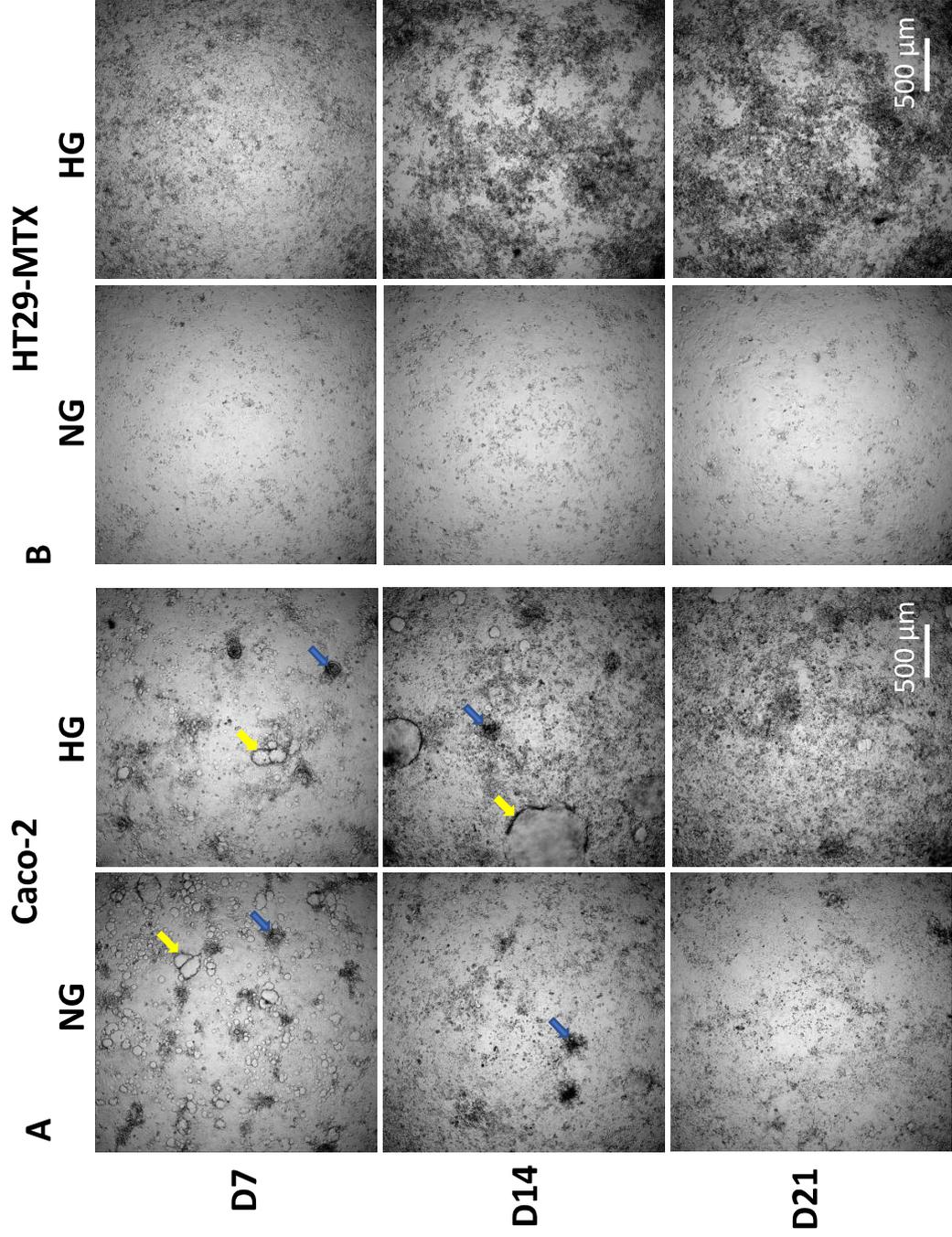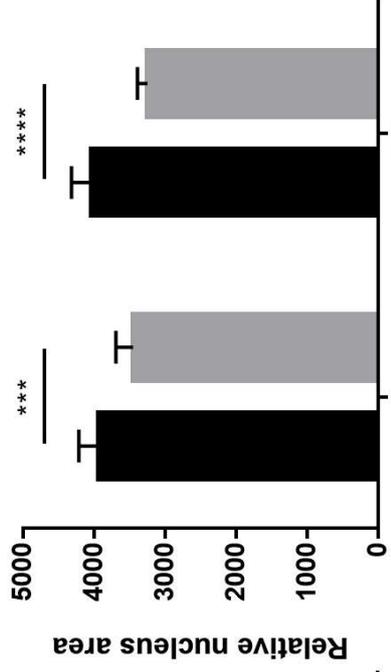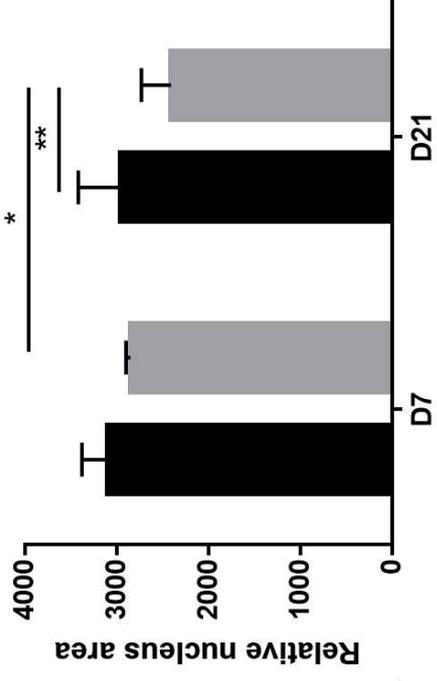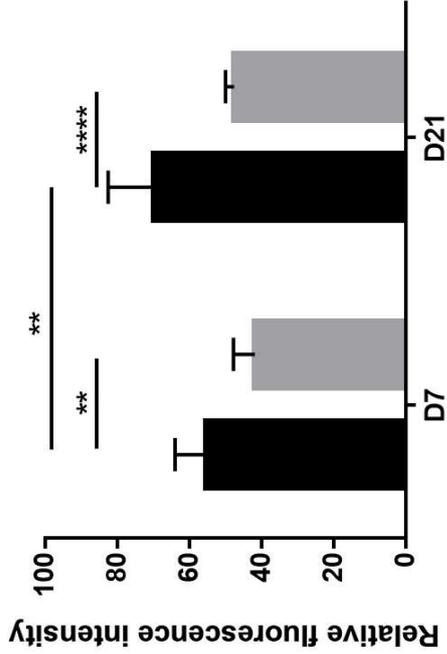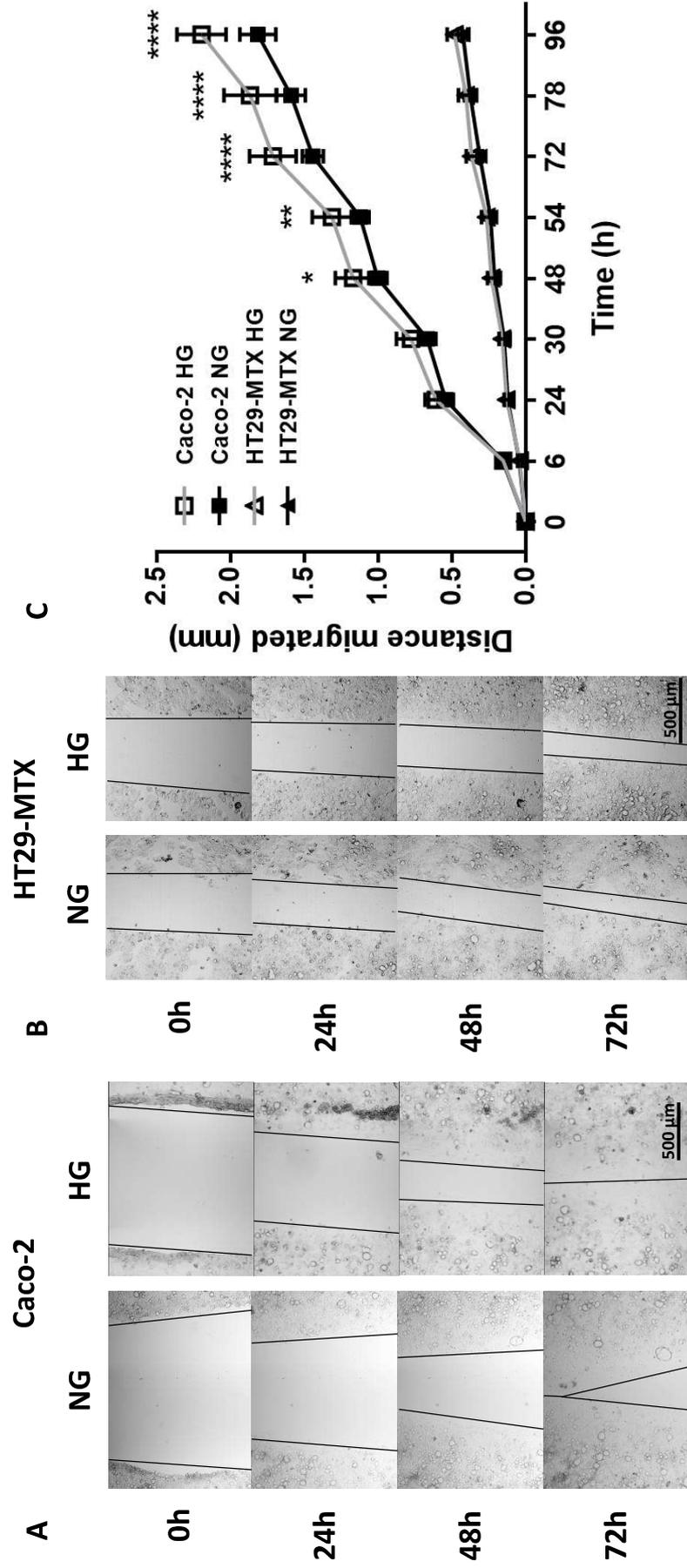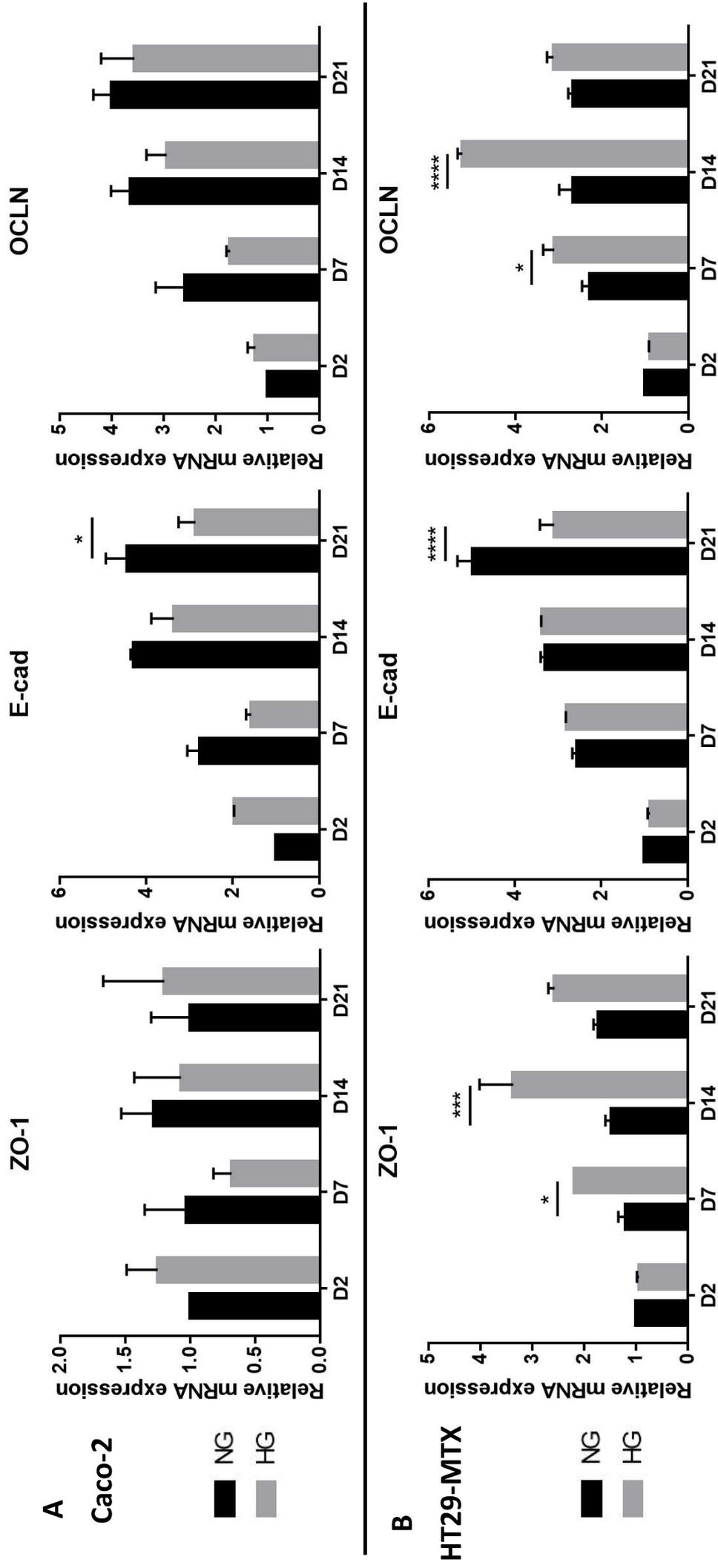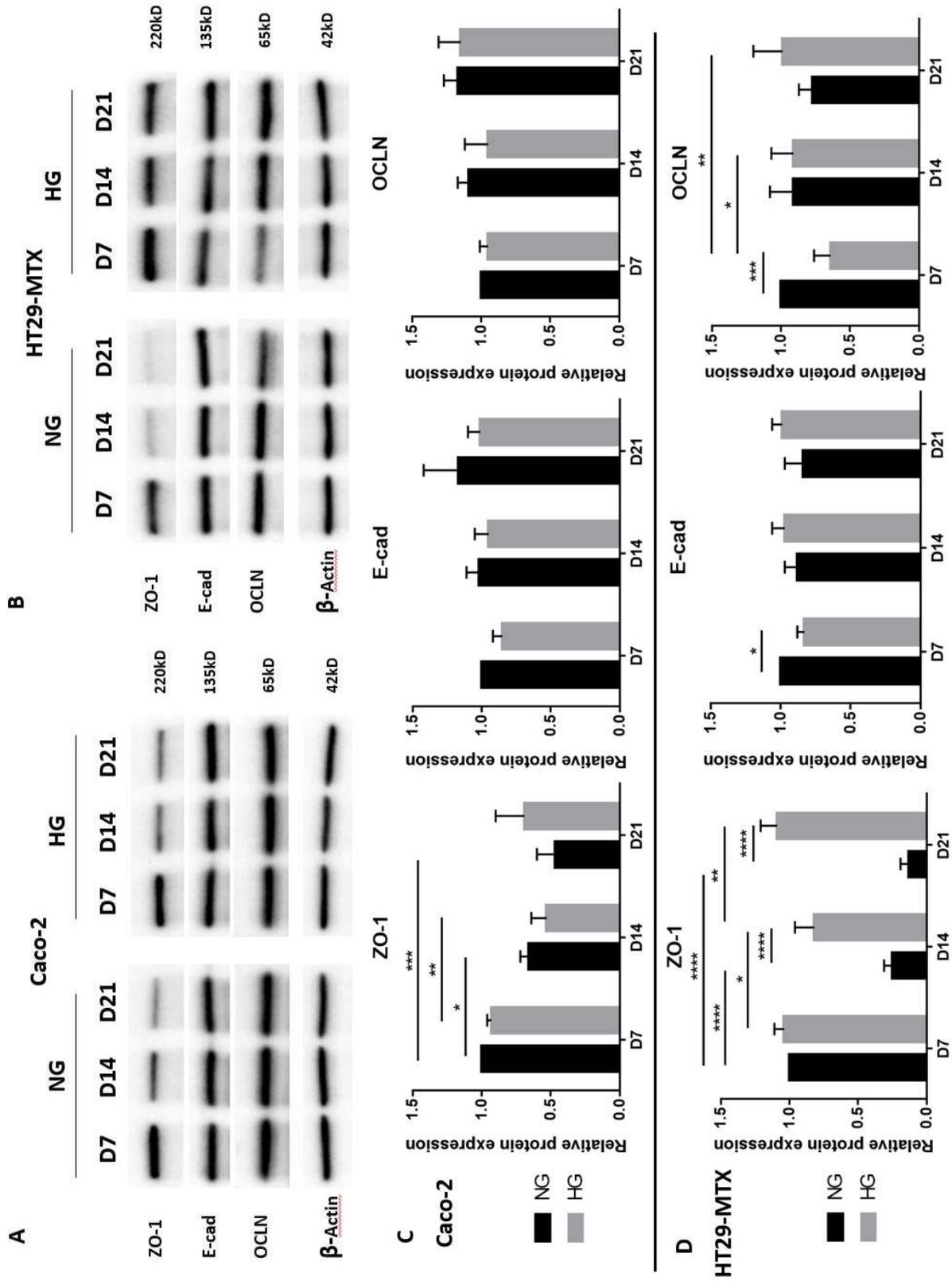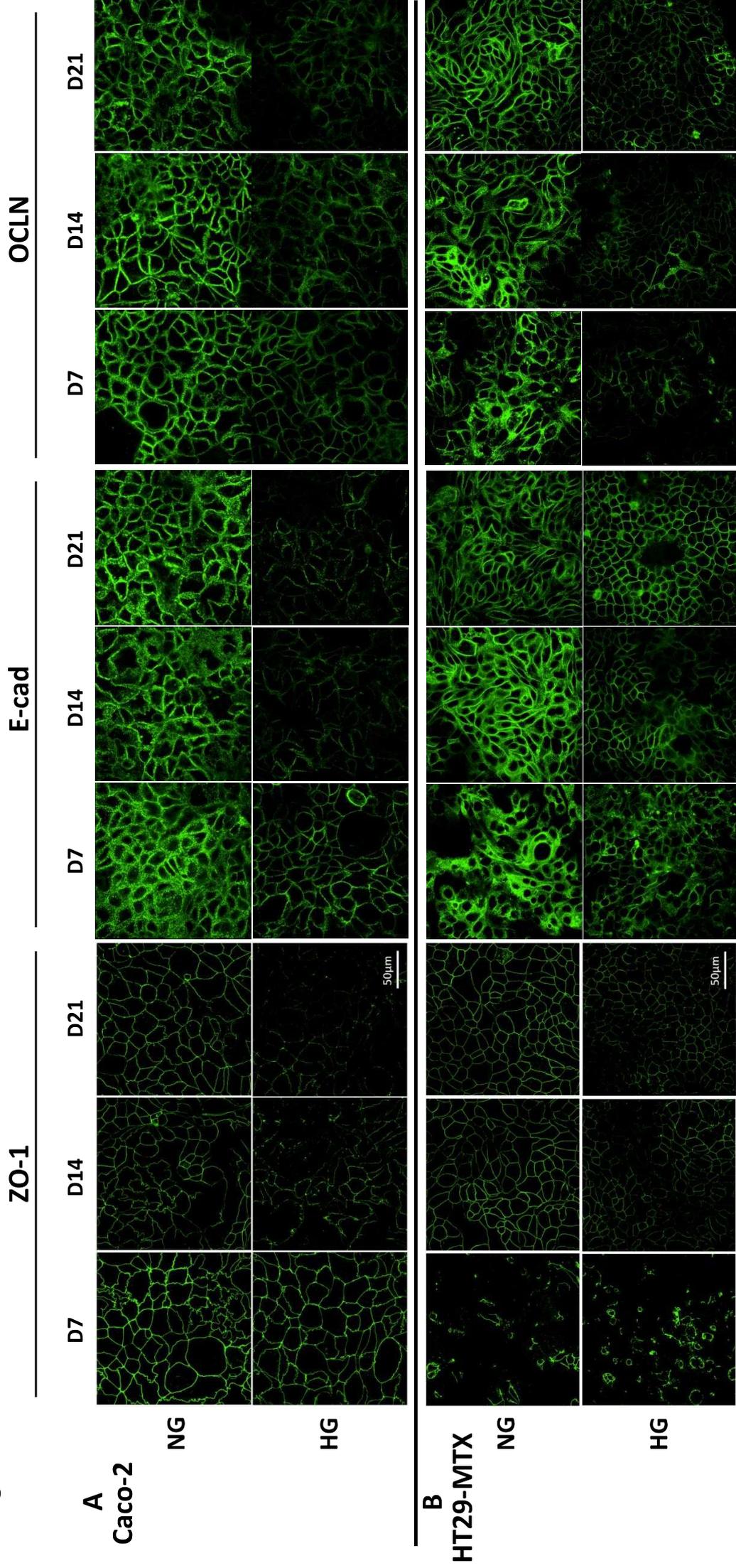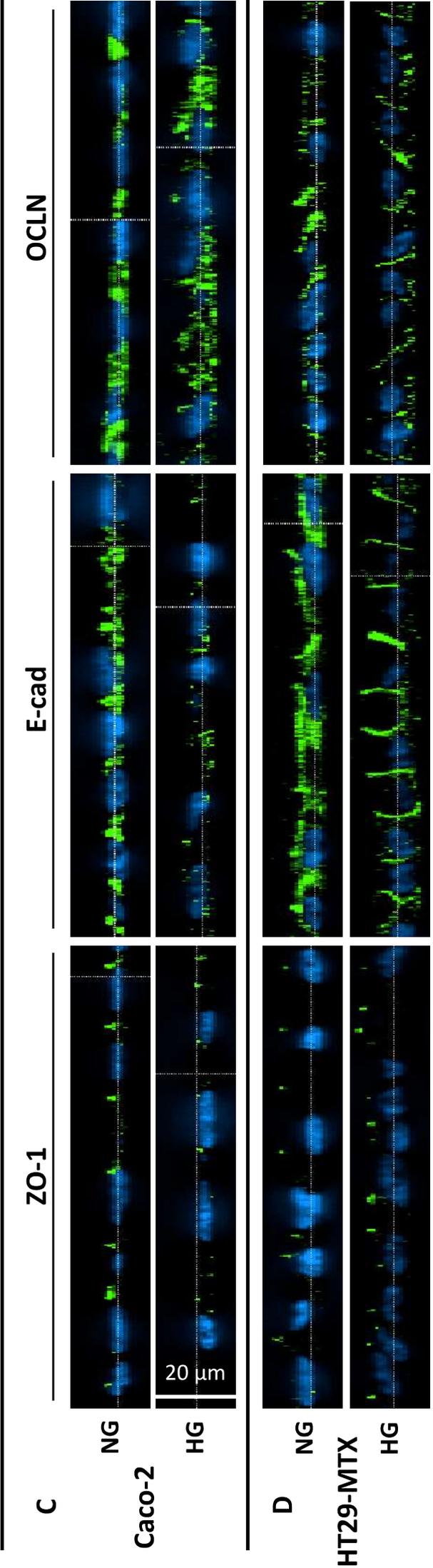| genes	Forward primer sequence (5'-3')	Reverse primer sequence (5'-3')	Product size
ZO-1	CAAGATAGTTTGGCAGCAAGAGATG	ATCAGGGACATTCAATAGCGTAGC	183 bp
OCLN	AAGAGTTGACAGTCCCATGGCATAC	ATCCACAGGCGAAGTTAATGGAAG	133 bp
E-cad	CTCGACACCCGATTCAAAGTG	CCAGAAACGGAGGCCTGATG	191 bp
Actin	CTGGAACGGTGAAGGTGACA	AAGGGACTTCCTGTAACAATGCA	140 bp

Figure-1

Figure-2

Figure-3

Figure-4
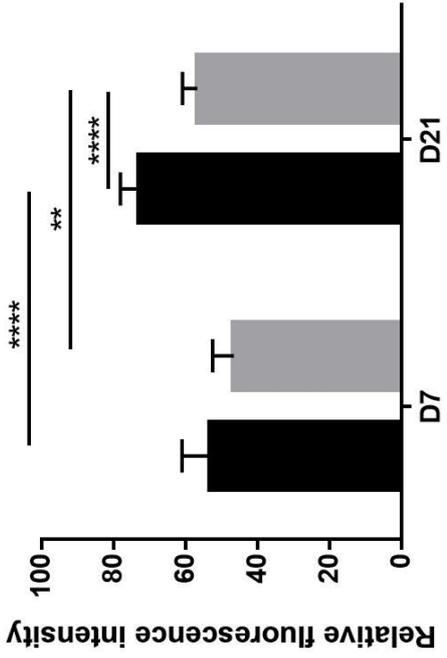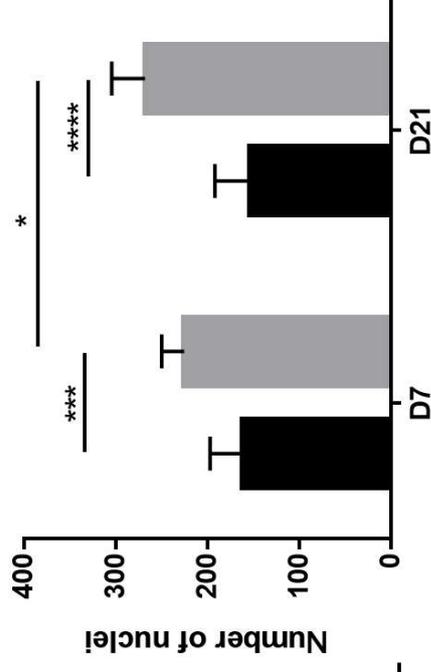
Figure-5

Figure-6

Figure-7

Figure-8

A Caco-2 — ZO-1 (D7, D14, D21), E-cad (D7, D14, D21), OCLN (D7, D14, D21); NG, HG

B HT29-MTX — ZO-1 (D7, D14, D21), E-cad (D7, D14, D21), OCLN (D7, D14, D21); NG, HG

50µm

Figure-8

C   Caco-2   ZO-1   E-cad   OCLN

NG

HG   20 μm

D   HT29-MTX

NG

HG

Figure-9

A

Caco-2   HT29-MTX

NG

HG

1 mm

B

% alcian blue staining area

100

50

0

Caco-2   HT29-MTX

NG
HG

C

HT29-MTX

NG

HG

50 µm

Figure-10

Figure-11